in Proceedings, University of Minnesota 50th Annual Geotechnical Conference (February 2002), pp. 21-84. J. F. Labuz and J. G. Bentler, Eds. Minneapolis: University of Minnesota.

Closing the Circle

Some comments on design procedures for tunnel supports in rock

C. Fairhurst [1]
C. Carranza-Torres [2]

Preamble

This overview has been prepared specifically for presentation at the 50th Annual Meeting of the Minnesota Geotechnical Society. Tunnel support design has been a subject of research at the University of Minnesota since the 1960's. It is also nearly half a century since Terzaghi (1946) proposed his method for tunnel support design in rock that was widely adopted in the United States. This paper provides an opportunity to illustrate the goal of rock mechanics research at 'Minnesota', that involves arriving at practical procedures through understanding of the basic physical principles that control the mechanical behavior of rock. Given the variability and unpredictability of geological materials, the 'numbers' resulting from calculations are considered to be of value primarily to the extent that they help elucidate these basic principles.

Introduction

The ancient art of tunnelling has evolved throughout history with occasional periods of impressive development, as in the Roman era and during the Industrial Revolution. At no time, however, have the demands on tunnelling developed as rapidly as during the last half century. Population growth, rapid urbanization, development of national and international rapid transportation networks, and a growing realization that many facilities built traditionally above ground can be located to advantage underground all combine to stimulate demand for tunnelling and underground excavation. Projects become more and more ambitious and important new problems appear, challenging the capabilities of the geotechnical engineer.

---

[1] Senior Consultant, Itasca Consulting Group, Inc. Minneapolis, Minnesota.
Professor Emeritus, University of Minnesota.
[2] Consulting Engineer, Itasca Consulting Group, Inc.

The advent of the high-speed computer and rapid developments in computing techniques over the past two to three decades together provide a potentially powerful tool to help the geotechnical engineer respond to this challenge. To use this tool effectively, however, it is essential to recognize the special characteristics of geological materials and the constraints imposed on design compared, for example, to problems involving fabricated materials. In the latter case, the mechanical response of the full-scale structure can be determined reliably from tests on small laboratory specimens. By contrast, a rock mass may contain joints, fractures, folds and other geologically-induced features such that the mechanical response of the full-scale structure may bear little or no relationship to the response of small scale specimens taken from the same mass. Further, the rock properties may vary considerably throughout a rock mass in a manner that, in many cases, cannot be determined from advance geological exploration.

In the case of tunnelling, concern is focused on the region affected by excavation of the tunnel face. Rock mass properties may change unexpectedly with each increment of tunnel advance. Narrow gouge-filled faults and comparable conditions, undetected in geological exploration, can produce dramatic changes in excavation stability. Less dramatic effects arise routinely as conditions change from those assumed in support design calculations. Labasse (1949), in discussing supports for tunnels in mines, summarized the situation as follows:

> *'First, the types of support to be used* [in the mine] *must be limited to one or two in order not to disrupt the material supply operations underground. This standardization makes precise calculation of a support for each section* [of tunnel advance] *useless. Further, the need to install the support immediately after excavation does not allow time to make calculations and fabricate the support. In order to arrive at a precise determination it would be necessary, in fact, to study each section separately because it would differ from neighboring sections with respect to the rock layers encountered, their dip and their disposition. It would be necessary to take a test specimen from each layer, determine its properties and the influence of these properties on neighboring layers. This would require a series of experiments and mathematical analyses whose solution, assuming that a solution is possible, would take up precious time during which the excavation would certainly have collapsed.'*

Thus, a good support design is one that *(i)* will stabilize the excavation for the conditions to be expected, and *(ii)* is capable of being adapted to deal with changes from these conditions as they are revealed at the face during excavation. [Note also that *time* is mentioned as a factor.] The terms *design as you go* and *the observational approach* are sometimes used to describe this method of design. For this approach to be successful, it is essential that the tunnel engineer know how to respond appropriately and quickly when the actual conditions are revealed —i.e. how to modify the design *on-site*, and how to establish that the changes have achieved

the desired effect. Thus, it is at least as important for the engineer to understand the general physics and nature of the mechanical changes produced in the rock in the vicinity of an excavation, as it is to know how to make the design calculations.

How, then, can numerical modelling techniques be used to best advantage to assist in tunnel support design? There appear to be several possibilities. In this paper, the authors examine two:

1. to assess the validity of current design approaches, most of which predate the 'computer age'; and
2. to extend the general insights on tunnel response, gained from classical analysis, to 'more practical' tunnelling situations.

The paper concludes with suggestions for further studies where numerical modelling could advance the 'state of the art' of tunnel support design.

Historical developments in mechanics relevant to tunnel support design

It is useful at the outset to review briefly the history of development of computational tools and solutions in mechanics, since tunnel support design has been guided in considerable measure by these developments.

The discovery of calculus in the second half of the 17th century by Newton and Leibnitz provided the direct stimulus for the development of continuum mechanics and the theory of elasticity. At the time, considerable attention was focused on attempting to arrive at the macroscopic behavior of materials by, in effect, the integration of interactions at the molecular scale. There was doubt and considerable debate as to the applicability of the continuum hypothesis, since it required the materials to have no discrete structure at the molecular level[1].

---

[1] One must mention the great difficulty in its development. Mathematical analysis in those days was built on the concept of continuous geometrical space in which it was possible to consider individual segments and to introduce the processes of differentiation and integration on this basis. The universally recognized Newtonian molecular theory of structure of bodies, on the other hand, represented them as discrete media composed of individual particles that are connected with each other by the forces of mutual attraction and repulsion. It proved to be very difficult to justify the applicability to such media of the apparatus of mathematical analysis, which was essentially connected with the concept of continuous functions capable of receiving indefinitely small (i.e. infinitesimal) increments, and with the possibility of passing to the limit in their summation (i.e., in their integration). On account of this, the first works on the mathematical theory of elasticity gave rise to much discussion; their validity was questioned. However, the fact that even an extremely small volume, presumably isolated from a body, contains a great number of molecules prompted investigators to appeal to the law of large numbers and to apply the method which was subsequently called statistical; this made it possible to bridge the gap between the continuous space of mathematical analysis and the solid body as a discrete medium. It became possible to apply the powerful apparatus of mathematics to the development of the new branch of physics.

'. . . doubts concerning the physical justification of the method of elasticity dealing, as it were, with a continuous solid medium, gradually disappeared. From this point

By the second half of the 18th century, however, continuum mechanics was established, together with the theory of elasticity and a number of important analytical elastic solutions had been obtained.

Solutions of particular relevance to tunnel support design are the Lamé (1852) solution for the stress distribution around a cylindrical or spherical cavity in an elastic medium subjected to uniform internal and external pressure and the Kirsch (1898) solution for stresses around a circular hole in an elastic plate subjected to biaxial loading. Inglis (1913) effectively extended the Kirsch result to consideration of an elliptical hole in an elastic plate. Figure 1 summarizes these results.

A very important feature of all of these analytical or closed form solutions is that the results are expressed in dimensionless form. Thus, the stresses are seen to vary as the square of the dimensionless ratio of the 'tunnel' radius [a] divided by the radial distance [r] —or as the cube of this ratio in the case of a spherical cavity— while the deformations are proportional to the ratio of the applied stress [σ] to the elastic modulus [E] of the medium. In the case of non-circular openings it is useful to recognize that the stress concentrations will tend to extend further behind the opening as the *local* radius of curvature increases[2]. These general results remain of significant value in current design, as will be noted below.

Many excavations in rock have profiles that deviate considerably from the simple geometries that are amenable to closed form analysis[3;4]. The development of Photoelasticity [Coker and Filon (1931); Frocht (1941)] provided an experimental technique to obtain very good estimates of the influence of complex excavation shapes on the stress distributions (Figure 2). Although two-dimensional photoelasticity was more common, three-dimensional analysis was also possible. As seen

---

of view, it is sometimes said that the theory of elasticity is based on the hypothesis of the continuous structure of solids. It must be borne in mind, of course, that this hypothesis is but a working hypothesis; it is dictated by the adopted mathematical method of investigation and does not intrude into the branches of physics that are directly concerned with the problems of body structure.' (Filonenko-Borodich, ca 1960).

'In the field of geomechanics, granular media and block-jointed rock masses are obvious examples where the concept of the ideal physical continuum —one in which no gaps are formed— cannot be expected to apply.' (Trollope, 1968, p. 275)

[2] This can be seen well in the photoelastic diagram of the stresses around the underground powerhouses in Figure 2b. The (shear) stress contours are very concentrated in the low radius regions (corners) and more extended in the high radius sections (walls).

[3] With the development of the Tunnel Boring Machine (TBM) the circular tunnel is now less of an idealization than in the past. The first TBM that successfully completed a tunnel was the Mitri Mole, used to excavate tunnels in the Pierre shale at the Oahe Dam site in 1955. A leading proponent of the TBM project at Oahe was the late Kenneth S. Lane, U.S. Army Corps of Engineers. The designer of the mole machine was J.S. Robbins, then a resident of St. Paul, Minnesota, who subsequently developed many TBMs for projects around the world, including the Channel Tunnel.

[4] Application of complex analysis allows some geometries other than circular to be studied (see for example, Savin 1961)

from Figure 2, the technique provided excellent graphical visualization of the stress distribution in the solid body. Obert and Duvall (1967) made extensive use of this technique to determine (and tabulate) stress concentrations around a variety of excavation shapes and the influence of adjacent excavations on the stress distributions. With the rapid increase in the power of computers and numerical techniques, such as the finite element method, interest in the photoelastic technique, which required careful experimental and interpretation procedures, declined. It is rarely used today.

Today numerical analysis is applied ubiquitously in engineering. In excavation problems analysis of realistic excavation shapes, including three-dimensional effects (e.g., the influence of the tunnel face on stability) and inelastic deformation of the rock mass can be performed readily. Frequently, however, these analyses are performed on a problem-by-problem basis, using the specific dimensions of the excavation and specific rock mass properties, with results listed in direct dimensional values. Although applicable to the particular situation considered, the general insights gained from the analytical approaches tend to be obscured. The authors believe that there is considerable merit in using numerical analysis to extend the analytical results in general form to explore practically interesting situations for which analytical results are not available. Some examples of this approach are presented below.

Several of the support design procedures developed in 'pre-numerical' times are still in use today. This paper comments briefly on five such methods[5]:

- Elastic Analysis;
- Terzaghi's Rock Load;
- Lang's Reinforced Rock Unit;
- Einstein-Schwarz's Flexibility/Stiffness Ratio;
- Convergence Confinement Method or
  New Austrian Tunneling Method (NATM)

Elastic Analysis

Clearly, if an excavation requires support, then the rock behavior does not remain elastic. While this is true, elastic analysis can provide considerable insight into support design. The expressions for elastic stress distribution in Figure 1, for example, show that the stress concentrations in the medium decrease as the ratio $(a/r)^2$ [where a is the tunnel radius, r is the radial distance] in the case of a cylindrical tunnel, and as $(a/r)^3$ in the case of a spherical cavity. This implies that the stress 'disturbance' ahead of the *elastic* front of a tunnel (assuming that it can be considered to approximate a hemisphere) will be limited to the order of $1.0 \sim 1.5$ tunnel radii ahead of the face[6] —i.e. $12\% \sim 4\%$ change in stress. Similarly, the effect of a cylindrical tunnel on

[5] Several empirical systems have also been developed, based on review and assembly of design data from a large number of completed tunnels, as design guides (e.g., Barton et al. 1974; Bieniawski 1976). These are not reviewed here.

[6] Note that the center of the hemisphere incorporating the tunnel face would be at a distance of one radius into the tunnel behind the face.

a)

Lamé (1852)

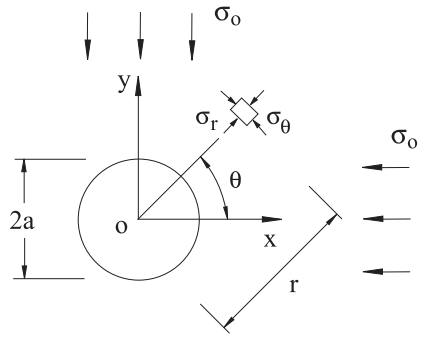

Cylinder

$$\sigma_r = \sigma_o\left(1-\frac{a^2}{r^2}\right)$$

$$\sigma_\theta = \sigma_o\left(1+\frac{a^2}{r^2}\right)$$

$$u_r = \sigma_o\frac{1+\nu}{E}\frac{a^2}{r}$$

Sphere

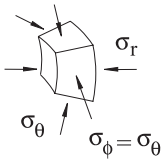

$$\sigma_r = \sigma_o\left(1-\frac{a^3}{r^3}\right)$$

$$\sigma_\theta = \sigma_o\left(1+\frac{1}{2}\frac{a^3}{r^3}\right)$$

$$u_r = \sigma_o\frac{1+\nu}{2E}\frac{a^3}{r^2}$$

b)

Kirsch (1898)

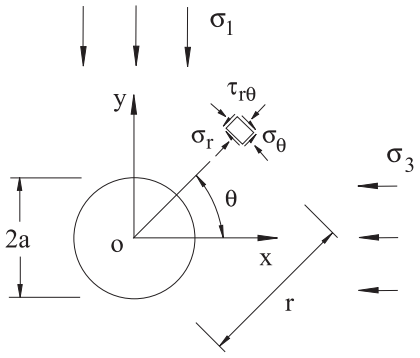

$$\sigma_r = \frac{\sigma_1+\sigma_3}{2}\left(1-\frac{a^2}{r^2}\right) - \frac{\sigma_1-\sigma_3}{2}\left(1-\frac{4a^2}{r^2}+\frac{3a^4}{r^4}\right)\cos 2\theta$$

$$\sigma_\theta = \frac{\sigma_1+\sigma_3}{2}\left(1+\frac{a^2}{r^2}\right) + \frac{\sigma_1-\sigma_3}{2}\left(1+\frac{3a^4}{r^4}\right)\cos 2\theta$$

$$\tau_{r\theta} = \frac{\sigma_1-\sigma_3}{2}\left(1+\frac{2a^2}{r^2}-\frac{3a^4}{r^4}\right)\sin 2\theta$$

c)

Adapted from Inglis (1913)

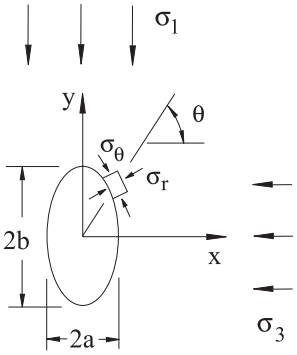

$$\sigma_\theta^{\text{wall}} = (\sigma_1+\sigma_3) - \frac{[(a-b)(\sigma_1+\sigma_3)+(a+b)(\sigma_1-\sigma_3)]}{a^2\sin^2\theta + b^2\cos^2\theta} \times \left(a\sin^2\theta - b\cos^2\theta\right)$$

Note: when $\frac{b}{a} = \frac{\sigma_1}{\sigma_3}$

then $\sigma_\theta^{\text{wall}} = (\sigma_1+\sigma_3)$ (constant)

Figure 1. Some classical solutions for holes in elastic medium.

a)

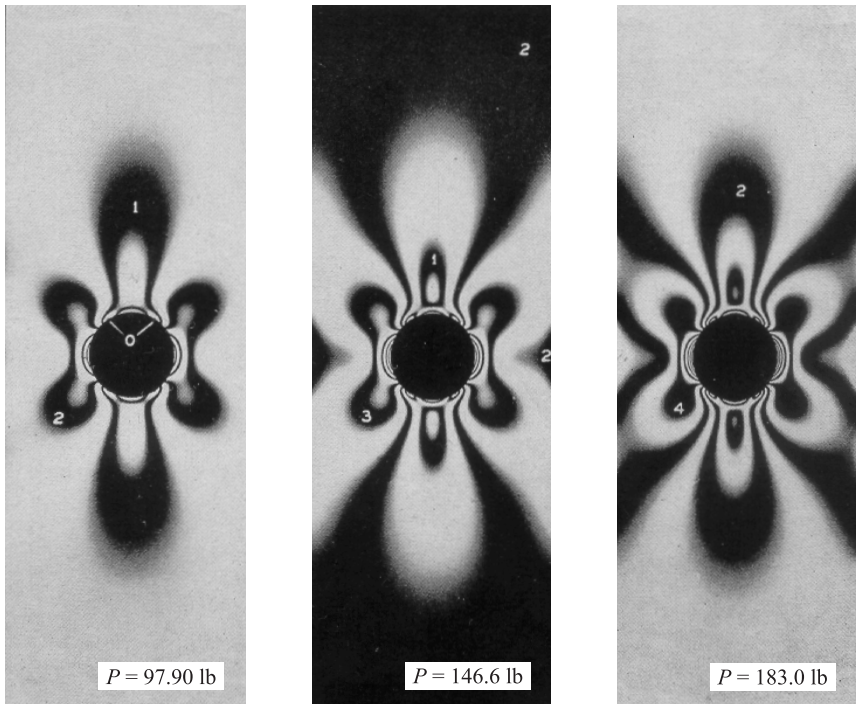

b)

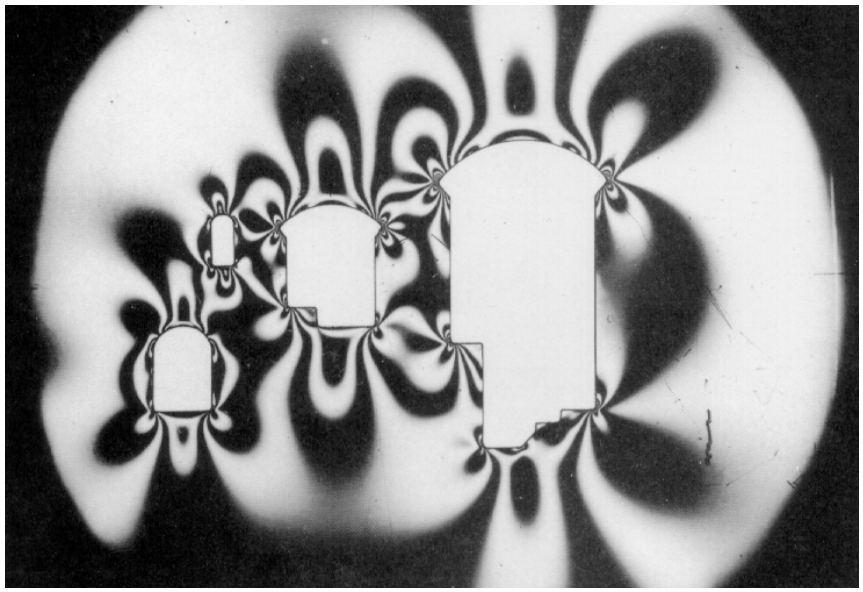

Figure 2. a) Stress patterns obtained from uniaxial tension of a plate cointaining a circular hole (after Frocht, 1941). b) Photoelastic model of excavations for a power house (after Lang, 1962).

changing the pre-existing state of stress in the vicinity of the tunnel will be minimal (11% $\sim$ 6%) beyond 3 $\sim$ 4 tunnel radii from the axis of the tunnel. Thus the loads imposed on two parallel tunnels of the same diameter placed with their centers say several tunnel radii apart can be considered to be independent of each other.

Figure 3 is a section showing the two main rail tunnels under the English Channel, with the smaller service tunnel parallel to and midway between them. It is possible to say at a glance that stresses around each of the main tunnels, spaced [$30/4.2 \simeq$] 7 tunnel radii apart will not be significantly different [$(1/7)^2 \simeq 2\%$] than the stresses around a single tunnel in the same rock. The service tunnel, distance about [$15/4.2 \simeq$] 3.6 large tunnel radii from the center of the large tunnels, will be subjected to an increase in loading of roughly $(1/3.6)^2 \simeq 8\%$ due to each larger tunnel —i.e. approximately 16% total increase in applied stress (the error in using superposition here is negligible).

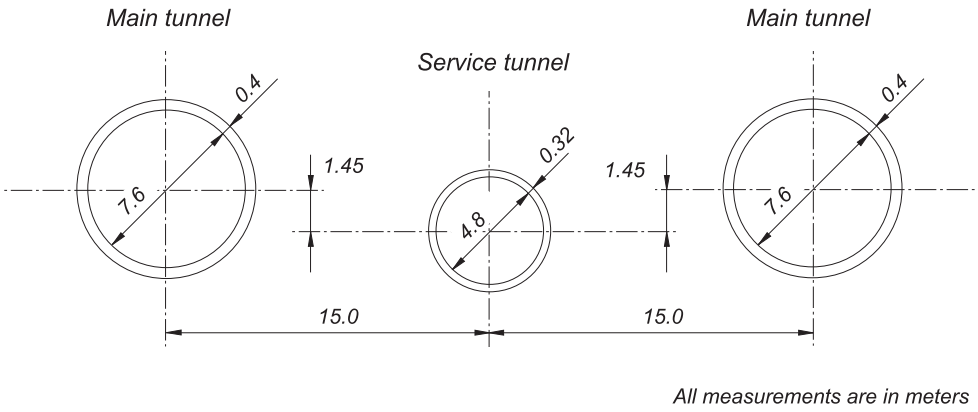

Figure 3. Typical cross-section of the railway tunnel system below the English Channel.

Elastic analysis (including photoelasticity) has been used to attempt to optimize the profile of excavations in competent rock. In the Kolar gold mines, near Bangalore, India, for example, an elliptical opening in which the *major:minor* axis ratio was the same as the *major:minor* stress ratio was considered to be the most stable shape [Isaacson (1958)], since the tangential stress was constant around the tunnel wall (Figure 1c). While this is true, examination of the stress distribution behind the periphery (Figure 5) reveals that the region of high stress is not constant [Carranza-Torres (1998)]. Thus, if the rock mass strength is lower than anticipated so that inelastic deformation develops, then the region of failure will not be uniform. As seen in Figure 5, analysis of the region of inelastic deformation indicates that rotation of the ellipse by 90° to the original orientation would result in a reduction of the inelastic region.

Analysis of the *elastic* stress distribution behind the tunnel periphery can provide a reasonable indication of where inelastic deformation is likely to develop in

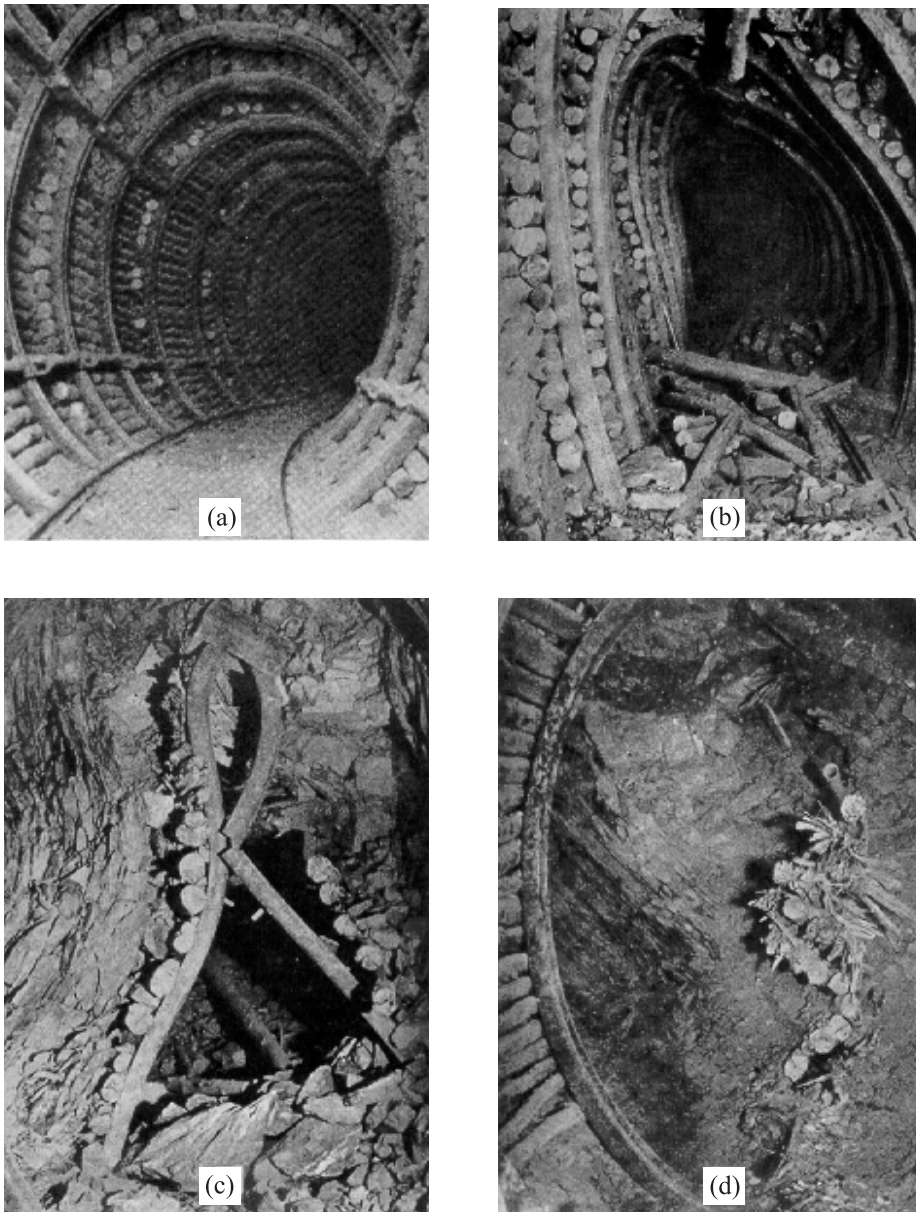

Figure 4. Damage to steel-setted drives due to rockburst in Champion Reef Mine (about 87 level), Kolar Gold Field, India (photographs reproduced from Caw, 1956).

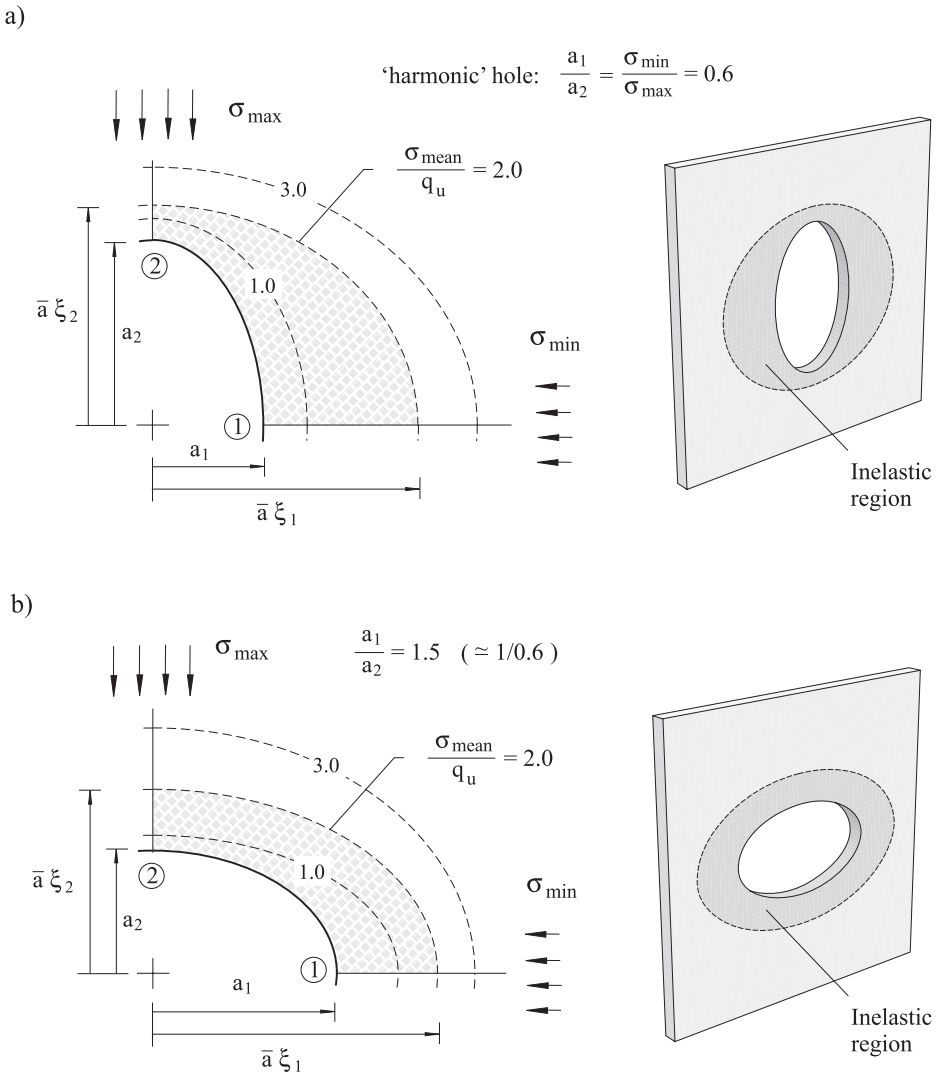

Figure 5. a) Boundary of inelastic region for the 'harmonic hole' [case $b/a = \sigma_1/\sigma_3$ considered in Figure 1c]. b) Failure pattern for the same elliptical opening rotated 90°.

the event that failure does occur. Elastic analysis is frequently used in this manner to provide a simple and informative 'first estimate' of the high stress regions where potential inelastic deformation may occur around excavations.

In the case of the excavations at Kolar, stress waves produced by rock bursting elsewhere in the mine resulted in overstressing and collapse of the excavations. As seen in Figure 4, the extent of collapse is consistent with the shape of the high stress region behind the periphery. [Note that the same shape of tunnel is being used to rehabilitate the tunnels; this is permissible, since the region behind the tunnel is now protected from future overloading by a destressed region.]

Elliptical tunnels designed on the same principle, termed the *'harmonic hole'* concept, were also proposed when the BWIP (Basalt Waste Isolation Project) site, now abandoned, in highly stressed basalt in Washington State was being considered by the U.S. Department of Energy as a potential repository for high-level waste. The effect of heat generated by the waste is an additional source of overstressing of the rock around repository excavations. Figure 6 shows the extent of the inelastic region due to heating of an harmonic hole that initially was in elastic state due to far-field stresses. It is seen that the inelastic region develops in a pattern similar to that in Figure 5a.

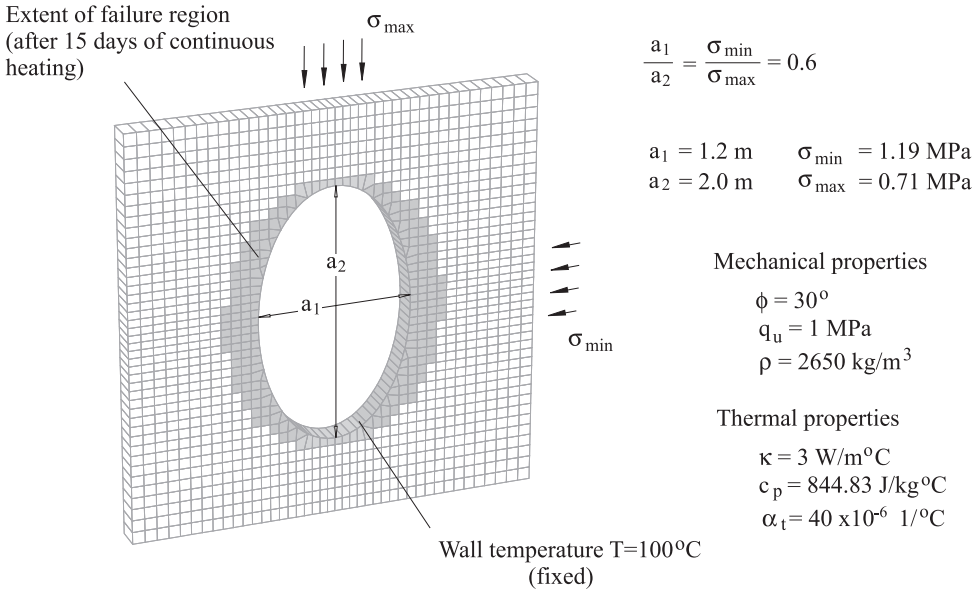

Figure 6. Inelastic region due to heating of an *harmonic* hole. Note that before heat is applied the problem is fully elastic; thereafter, the inelastic region develops as in Figure 5a.

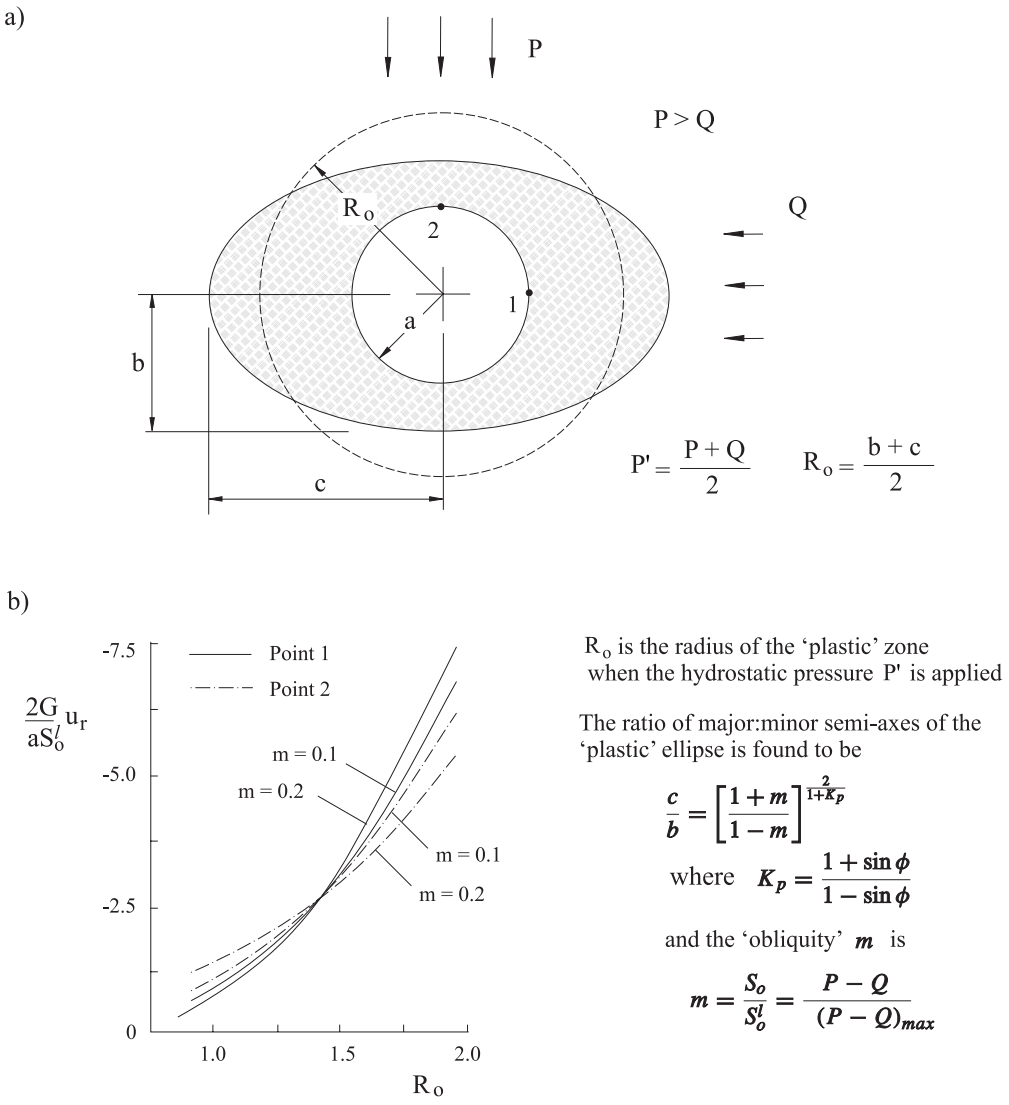

Figure 7. Inelastic zone around a circular tunnel for the case of non-uniform far-field stresses (after Detournay, 1983).

Elasto-Plastic Analysis

Analytical extensions of Lamé's elastic solution to include plastic deformation around the cavity have been worked out by numerous authors for a variety of assumed models (e.g., Tresca, Mohr- Coulomb, dilatational and non-dilational models) of the plastic behavior of the material. Probably one of the most elegant and comprehensive analyses is that by presented by Salençon (1969). Most (pre-numerical) discussions of inelastic deformation around tunnels start from these solutions, all of which, of course, are restricted to the special case of uniform far-field stresses (i.e., the Lamé's case of Figure 1a).

Detournay (1983) has considered what is, in effect, the elasto-plastic extension of the Kirsch solution (i.e., the case where the far-field stresses are non uniform as in Figure 1b) and has obtained a semi-analytical solution for the stress and displacements around a circular cavity. This is an important development, since many practical situations in rock mechanics involve non-uniform far-field stresses.

Figure 7a shows the elliptical pattern of inelastic deformation obtained. It is found that the mean radius R_o of the elliptical region is equal to the average of the major and minor semi-axes of the ellipse; that the major extension of the plastic zone is normal to the direction of the maximum far-field stress; and that the point of maximum displacement (Figure 7b) is located initially at the point (2) on the wall along the axis parallel to the maximum stress but changes to the point normal to the maximum stress direction as the radius R_o increases —i.e., to the point (1) indicated in Figure 7a. Although the solution is limited to certain values of stress difference $(P - Q)$, characterized by the 'obliquity' m, numerical studies confirm the same general behavior for greater stress differences.

Terzaghi's Rock Load Design

The Terzaghi (1946) rock load design method has been a standard procedure for civil engineering tunnels in the U.S. since it was introduced over 50 years ago. To establish the method, Terzaghi considered the case of a rectangular tunnel (supported by wooden posts) excavated through *'... a bed of sand...'* as shown in Figure 8a. In Terzaghi (1943), he states:

> *'... the cohesion of the sand is assumed to be not in excess of the feeble bond produced by a trace of moisture...'*
>
> *'Owing to the imperfect fit of the timbers at the joints and the compressibility of the supports of the footings of the vertical posts, the yield of the timbering is usually sufficient to reduce the pressure of the sand on the timbering almost to the value corresponding to the state of incipient shear failure in the sand. This state is similar to the state of stress in a mass of sand above a yielding strip. The sand adjoining the sides of the tunnel also subsides on account of the yield of its lateral support. The inclined boundaries of the zone of subsidence rise at an angle of* $45° + \phi/2$*. Therefore, at the level of the roof of the tunnel, the width of the yielding strip is approximately equal to*

$$2B_1 = 2[B_o + H \tan(45° - \phi/2)] \qquad (1)$$

He then assumes that the yielding region extends vertically upwards from points b_1–b_1 at the level of the roof (see Figure 8a) and from this situation, he computes the vertical pressure on the horizontal section b_1–b_1 to be

$$\sigma_v = \frac{\gamma B_1}{K \tan\phi}\left(1 - e^{-K \tan\phi \; D/B_1}\right) \qquad (2)$$

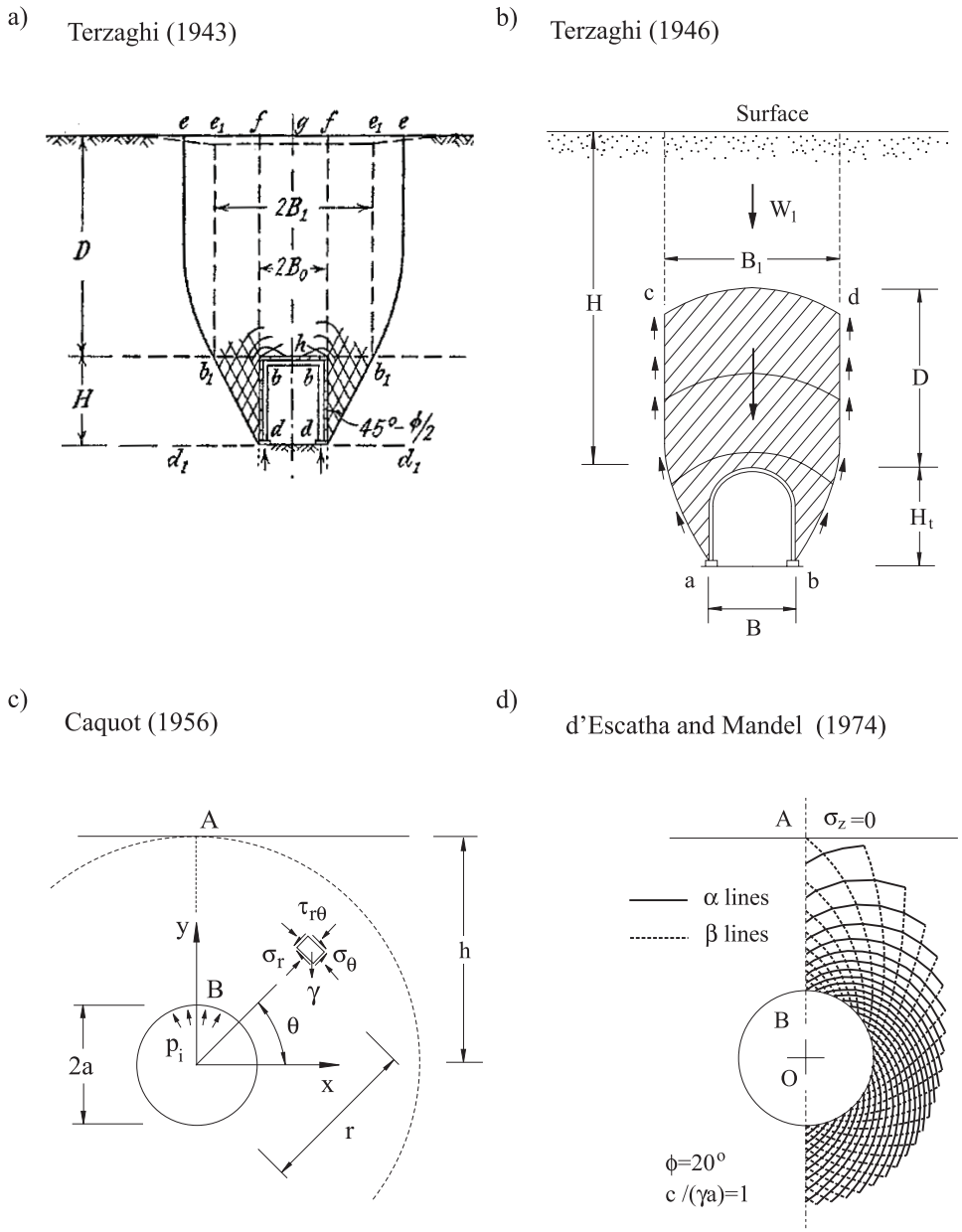

Figure 8. Some classical analytical solutions for the analysis of stability of shallow tunnels.

where K is an empirical coefficient he founds to be close to one[7].

Caquot (1956) and d'Escatha and Mandel (1974) have analyzed essentially the same problem studied by Terzaghi, using more rigorous upper bound analyses. In this approach statically admissible stress fields are constructed to establish a value of the support pressure that must be applied to the periphery of the (circular) tunnel to ensure that it will remain in static equilibrium —i.e., the actual pressure at which the tunnel would collapse will be lower than the upper bound value calculated from this theory. The two situations are illustrated in Figures 8c and 8d. [Note that d'Escatha and Mandel (1974) present the upper bound pressure values (for various friction and cohesion values) in graphical form only; Caquot (1956), on the other hand, provides closed-form expressions to compute these values.]

A comparison of the predicted tunnel support pressure required for tunnels of different depth (and similar soil conditions) for each of the methods discussed in Figure 8 is shown in Figure 9a. It is seen that the values predicted by the Terzaghi method are considerably higher than the other two.

As noted above, the upper bound estimates should result in a pressure above the value at which the tunnel would start to fail. To check this, the finite difference numerical code FLAC was used to simulate the effect of progressively reducing the support pressure on the wall of the circular tunnel until failure was induced. The procedure is summarized in Figure 9b. The figure shows the model corresponding to a circular tunnel located at a depth equal to three times the radius of the tunnel. The internal pressure is decreased in steps from the upper bound value given by d'Escatha and Mandel, until equilibrium of the model is not possible anymore.

For example, Figure 10 shows several stages during failure development as the support pressure is reduced. It is to be noted that failure did not start until the pressure was reduced to [$0.55/0.7 \simeq$] 80% the upper bound value calculated by Caquot and d' Escatha and Mandel solutions.

It is perhaps worth noting that the classical manual 'Rock Tunneling with Steel Supports' (Terzaghi 1946) provided a table of estimated dimensions of 'broken ground' above the tunnel for various rock conditions —the shape of the broken zone is the one shown in Figure 8b and it is similar to the one obtained with numerical models in Figure 10. The values were apparently based on observations of the degree of crushing of wood blocking above steel supports in a number of tunnels. The table has since been modified to reduce the load values by Deere et al. (1969).

Lang's Reinforced Rock Arch Design (1961)

Lang questioned the logic of installing a concrete arch lining in underground excavations for underground hydroelectric power plants, when the strength of the rock being excavated was comparable to that of the concrete. The reason was, of course, the probable existence of joints and fractures in the rock mass that may reduce the

[7] Equation (2) is derived on essentially the same basis as that used by Lang in determining the effect of bolts in creating his Rock Reinforcement Units (RRU's) —see equation (A-5) in Appendix A.

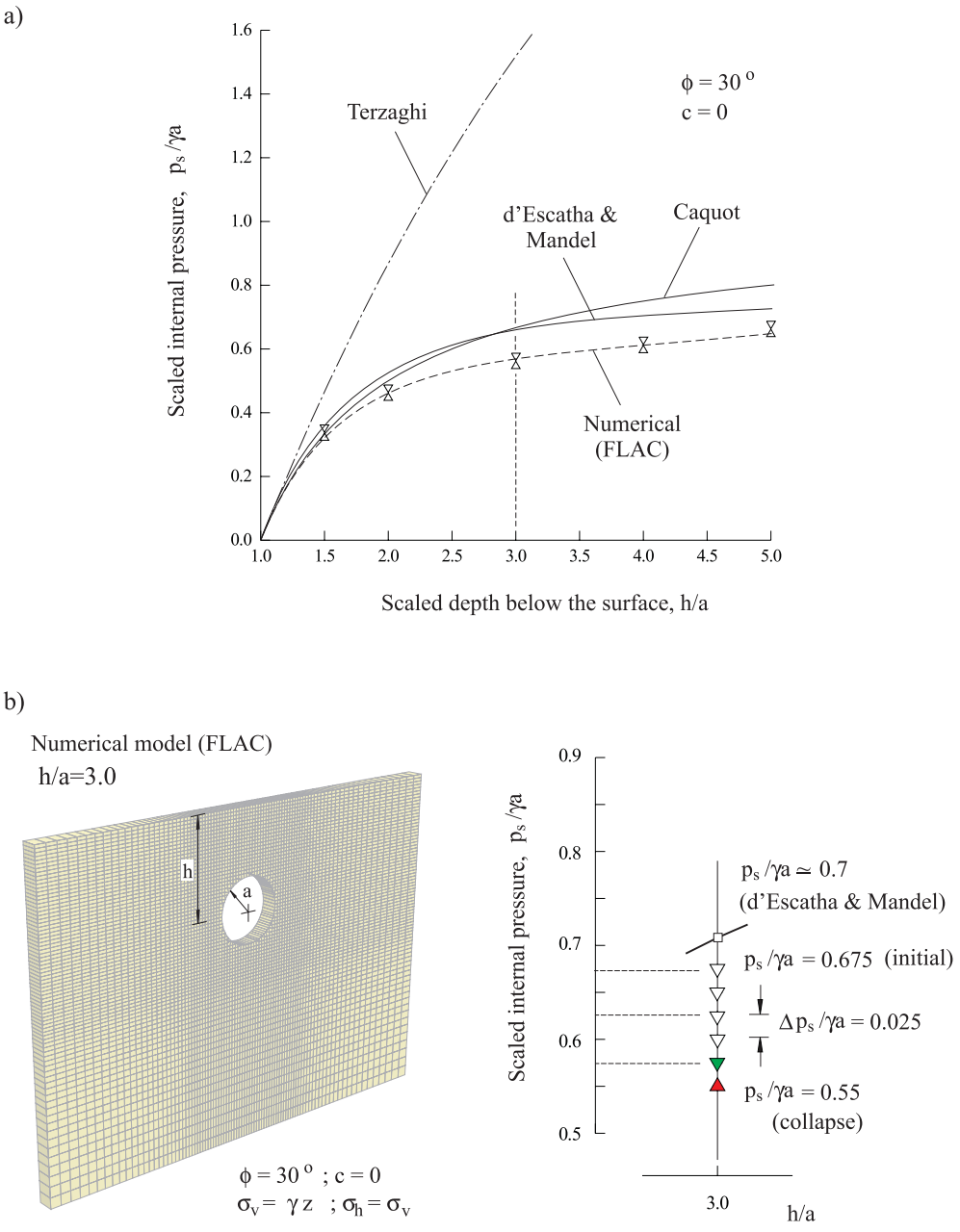

Figure 9. a) Comparison of the required support pressure obtained with the different models in Figure 8. b) Numerical model used to determine the 'actual' value of internal pressure required for equilibrium.

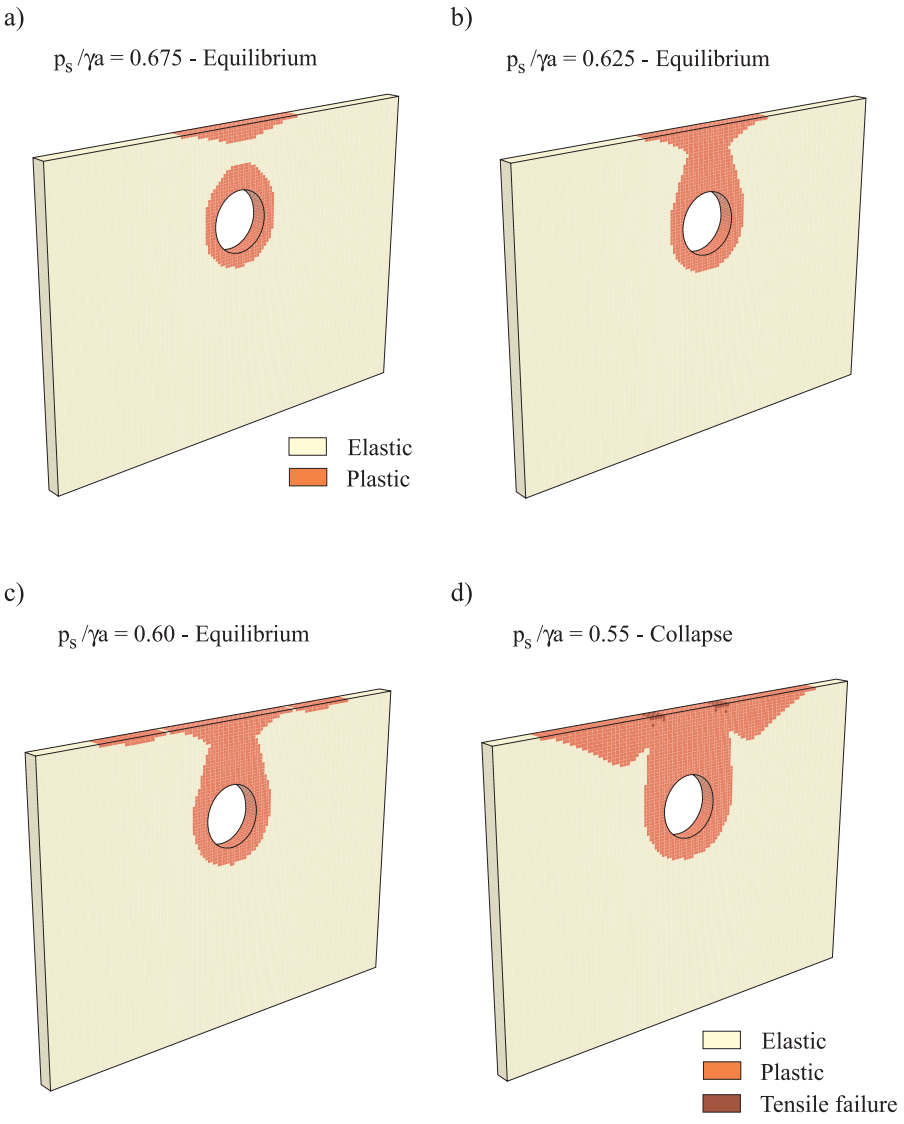

Figure 10. Sequence of decreasing internal pressure that leads to the 'collapse' of the tunnel in Figure 9b (results obtained with FLAC).

strength considerably. These fractures do not exist in the concrete. Lang proposed to overcome this problem by creating, in the roof of the excavation, an arch region within which any fractures would be 'locked together' sufficiently so that the arch would be stable. Locking would be obtained through a system of rock bolts in the roof. Although rock bolts were in use for temporary support of mine roadways, Lang pioneered their use in large civil excavations.

Lang's design seeks to create a system of reinforced rock units (RRU's) in the roof (see Figure A-1 in the Appendix A), creating an arch that is assumed to be free-standing and capable of supporting a region of 'distressed rock' above the arch (the weight of the arch is included as part of the total load to be supported by the arch). Lang used the Terzaghi Rock Load approach (Figure 8a) to determine the magnitude of the load to be transmitted to the bolt.

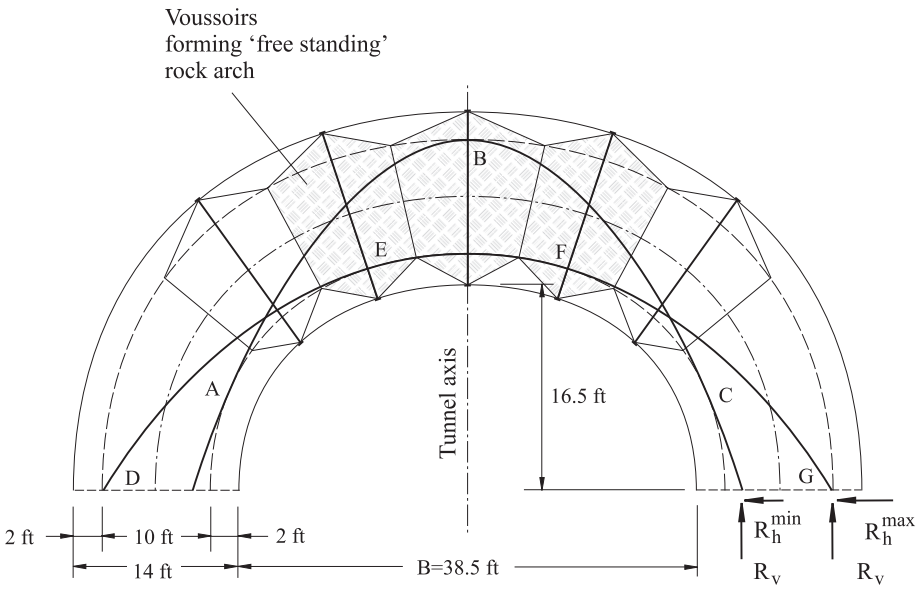

Figure 11. 'Voussoir' arch formed by reinforced rock units (after Lang, 1961).

The principle of the RRU is illustrated in Appendix A where the calculation for an *unreinforced* rock unit (i.e., no rock bolt is installed as shown in Figure A-1b) is presented in detail. In this case, the calculation determines the minimum support needed at the lower face of the unit to prevent collapse/fallout of the unit. This passive support could be provided, for example, by a simple prop. Lang then calculates the effectiveness of a simply anchored bolt (Figure A-1c) in providing the required passive support. The paper Lang and Bischoff (1984) contains a detailed discussion of this method, including analysis of grouted and pretensioned bolts. It is shown, for example, that the optimum reinforcement is achieved with a bolt length $[L]$ that is not more than three times the bolt spacing.

Bolting across the roof of an excavation in accordance with these rules, he creates a reinforced arch. Each of the RRU's is considered to act in a manner analogous to the masonry voussoirs in classical masonry arch construction (as represented schematically in Figure 11). Invoking design rules established by Coulomb (1776) —see Heyman (1972)— Pippard et al. (1939a, 1939b, 1941) and Kooharian (1952), Lang defines a zone of uniform lateral compression (developed by the bolting) in the central region of the arch. Under an (assumed) uniformly distributed load of distressed rock above the arch, the thrust line is parabolic. Figure 11 shows the RRU voussoir arch and the limiting parabolic thrust lines [*DEFG*; *ABC*]. Provided the thrust line is fully contained within the reinforced voussoir ring, the actual (parabolic) arch is everywhere in compression and will be stable (details of the computational procedure are described in Lang and Bischoff 1984).

Although the authors have not yet completed a numerical analysis of Lang's method, it appears that it has a number of conservative features in common with Terzaghi's method. The rock mass is not a free standing arch, and hinge failure (the reason for restriction of the thrust line location) is not likely in the rock mass. Study of the Lang method and comparison with the convergence-confinement load prediction for the same reinforcement system is continuing.

Einstein-Schwartz Flexibility/Stiffness Design (1979)

The design procedure proposed by Einstein and Schwartz (1979) is very similar to the Ranken and Ghaboussi (1975) method described in the ASCE Guidelines for Tunnel Lining Design (see American Society of Civil Engineering 1984).

The problem examined is that of support design for a circular tunnel in rock subjected to unequal principal in-situ stresses in the plane perpendicular to the axis of the tunnel (Figure 12a) —i.e., the problem is similar to that considered by Kirsch (1898), but in this case deformation of the hole is constrained by an elastic annular ring representing a liner.

Einstein and Schwartz assume, in essence, that the circular support is installed in intimate contact with the rock *before* the in-situ stresses are relaxed (i.e., before the tunnel is excavated, and that the full in situ stresses are applied to the support). Several situations are examined, e.g., conditions of *i)* a smooth (frictionless) or *full-slip* interface; *ii)* a rough, or *no-slip*, rock-support interface. The real situation will lie between the two, so that examination of the two extremes should serve to bound the loads on the support[8].

[8] The assumption that the support is subject to the effect of the full in situ stresses would appear, at first sight, to be conservative since, in reality, some initial deformation of the rock will occur before the support can be installed.

The above situation is, however, oversimplified since rock, when exposed to the tunnel environment (e.g., stress concentrations, air, moisture, etc.), tends to degrade progressively with time. The empirical *Stand-Up Time* rule (Lauffer 1958), for example, provides estimates of the length of time that an excavation can stand unsupported before collapse —depending on rock type, jointing, size of excavation, groundwater conditions, etc. The degradation processes will occur, at least to some

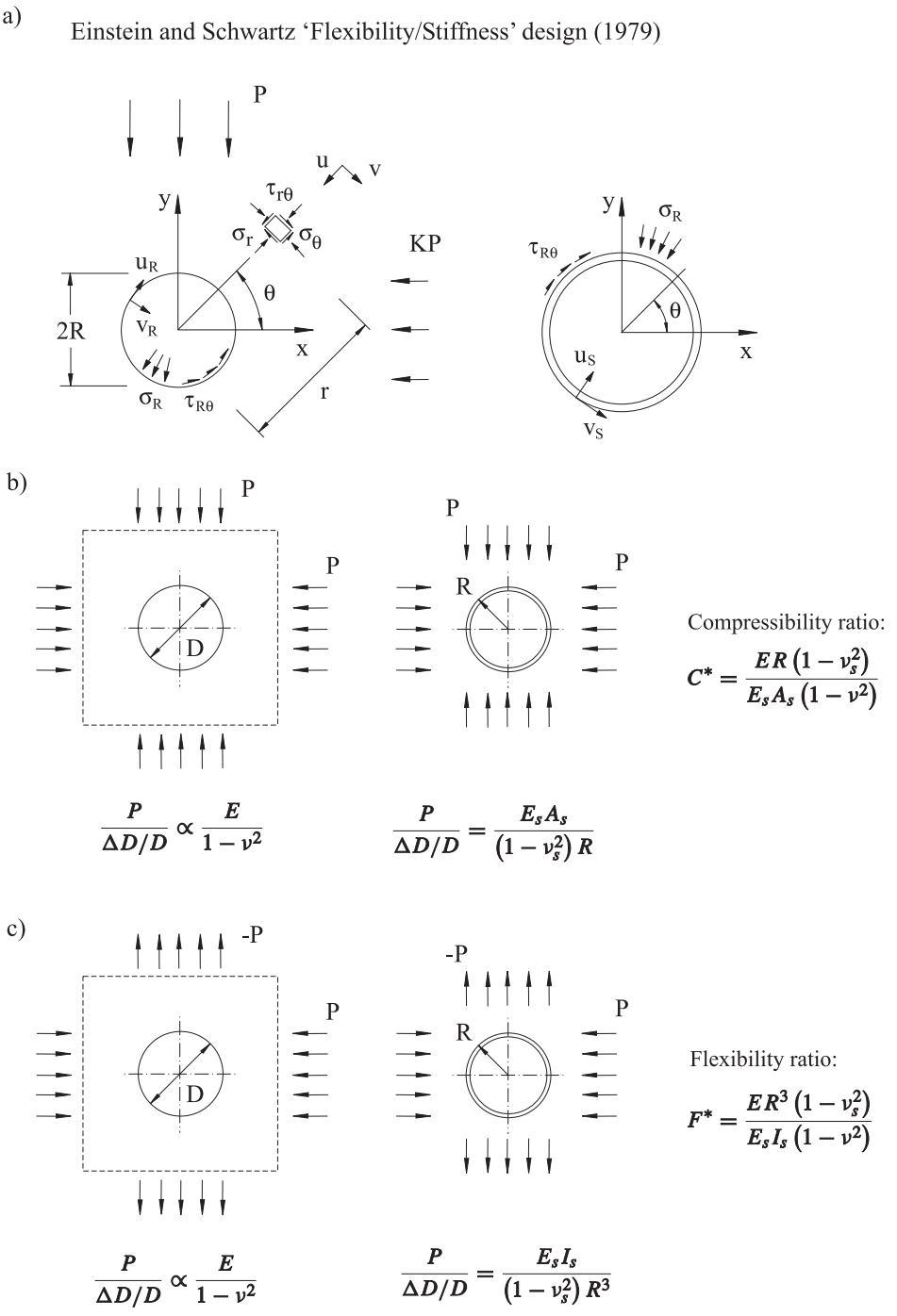

Figure 12. Rock-support elastic interaction problem considered by Einstein and Schwartz (1979).

In the Einstein and Schwartz solution, the variation in thrust and bending moment on the support is expressed in terms of two dimensionless parameters, the *Compressibility ratio* [C^*] and the *Flexibility ratio* [F^*] —see Figures 12b and 12c. For a given support, these ratios are determined essentially by the stiffness (or deformability) ratio of the rock mass and the support [E_r/E_s] —which has been used in our study as the basis for comparison of results.

In our study we have examined the implications of inelastic deformation produced by the applied stresses on the predictions of the Einstein and Schwartz support design. The problem is formulated in terms of dimensionless variables similar to those used by Einstein and Schwartz in order to retain the valuable attribute of ease of assessment of the effect of variability (uncertainty) in rock properties. Since we now consider inelastic deformation of the rock-mass, we need also to define a criterion of failure for the rock-mass. This was not required in the original analysis by Einstein and Schwartz, since the rock-mass was assumed not to fail.

The problem considered in our analysis is shown in Figure 13a. The figure represents a section of circular tunnel of radius R lined with a closed annular support of thickness t_s —the support is considered to be elastic with a Young's modulus E_s and a Poisson's ratio ν_s. The rock-mass is assumed to satisfy the Hoek-Brown failure criterion (the 'failure zone' indicated in Figure 13a corresponds to rock that has undergone plastic deformation according to this criterion). In particular we have used a scaled form of the Hoek-Brown failure criterion originally proposed by Londe (1988). [A detailed discussion of the Hoek-Brown failure criterion and this particular form of scaling is included in Appendix B.]

The tunnel is assumed to be deep enough that variation of vertical loading across the height of the excavation can be ignored. The far-field stresses are defined by the principal stresses σ_h in the horizontal direction and σ_v in the vertical direction. The stress state is characterized by a *mean* stress σ_o and a horizontal-to-vertical stress ratio k,

$$\sigma_o = \frac{\sigma_h + \sigma_v}{2} \qquad\qquad k = \frac{\sigma_h}{\sigma_v} \tag{4}$$

---

extent, even in the presence of support, so loading of the support will occur with time.

An approach sometimes used in support design to account for this degradation process is to define a long-term modulus of the rock, E_r^t, by the empirical expression

$$E_r^t = \frac{E_r^i}{1 + F(t)} \tag{3}$$

where $F(t)$ is some arbitrary function that results in a specified reduction of the instantaneous modulus over the long term. Thus, E_r^t may be taken as some fraction (say $0.1 \sim 0.3$) of E_r^i depending on the rock and the judgment of the designer. This approach has been discussed by Muir Wood (1975). Thus, a 'pseudo-elastic' loading after installation of the support can be postulated as appropriate for use in the Einstein and Schwartz method. In reality, however, this progressive rock degradation implies irreversible or inelastic degradation. Given that the Einstein and Schwartz method considers the situation in which the applied (in-situ) rock stresses are unequal (i.e., *non-hydrostatic*), it seems probable that the degradation would also vary with angular orientation around the support. The loads imposed on the support due to the degradation would thus be similarly non-uniform.

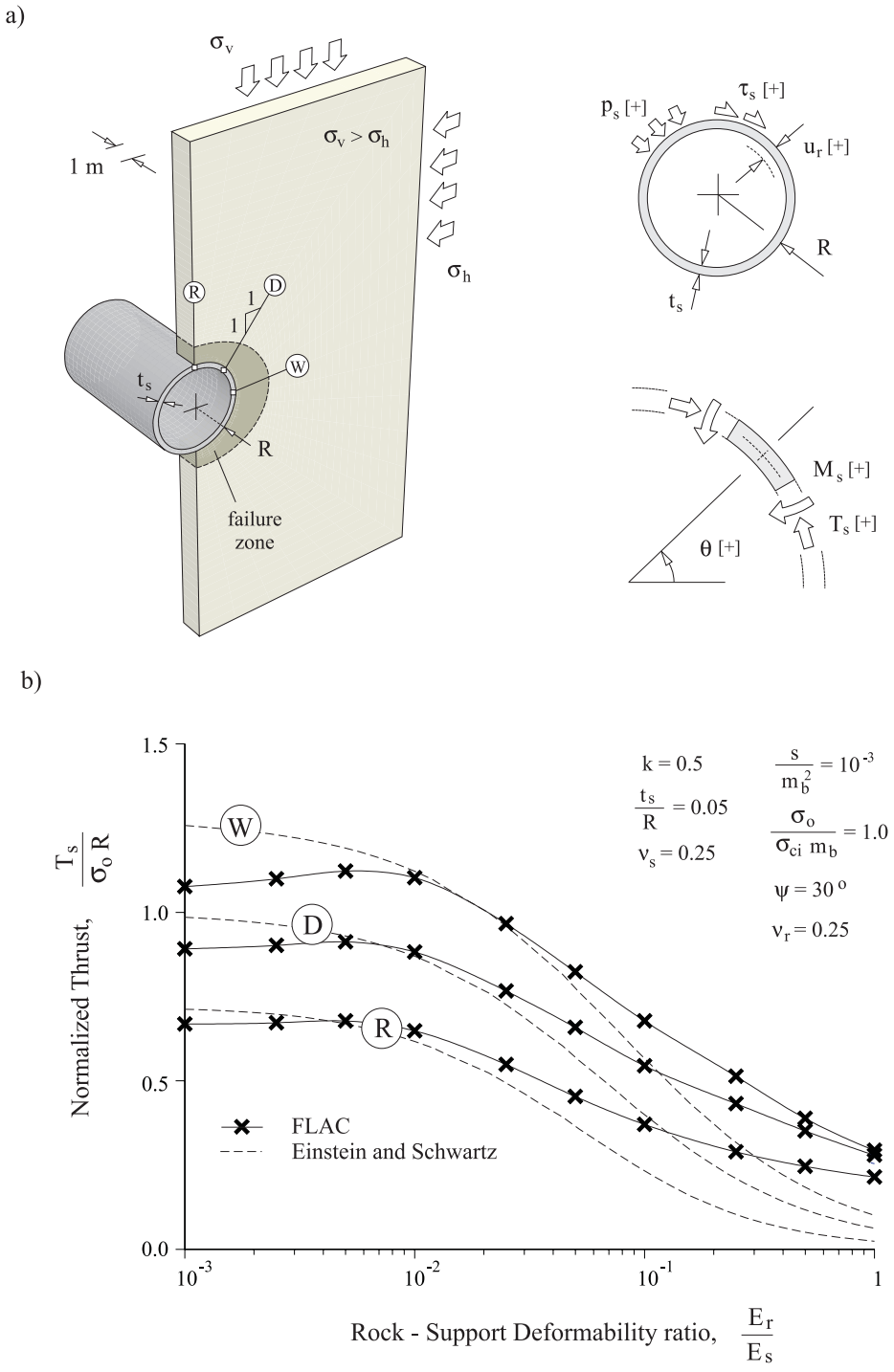

Figure 13. a) Section of lined tunnel in inelastic material, subject to non-uniform far-field stresses. b) Comparison of thrust distribution on the lining as obtained with Einstein and Schwartz (1979) elastic solution and with elasto-plastic numerical models.

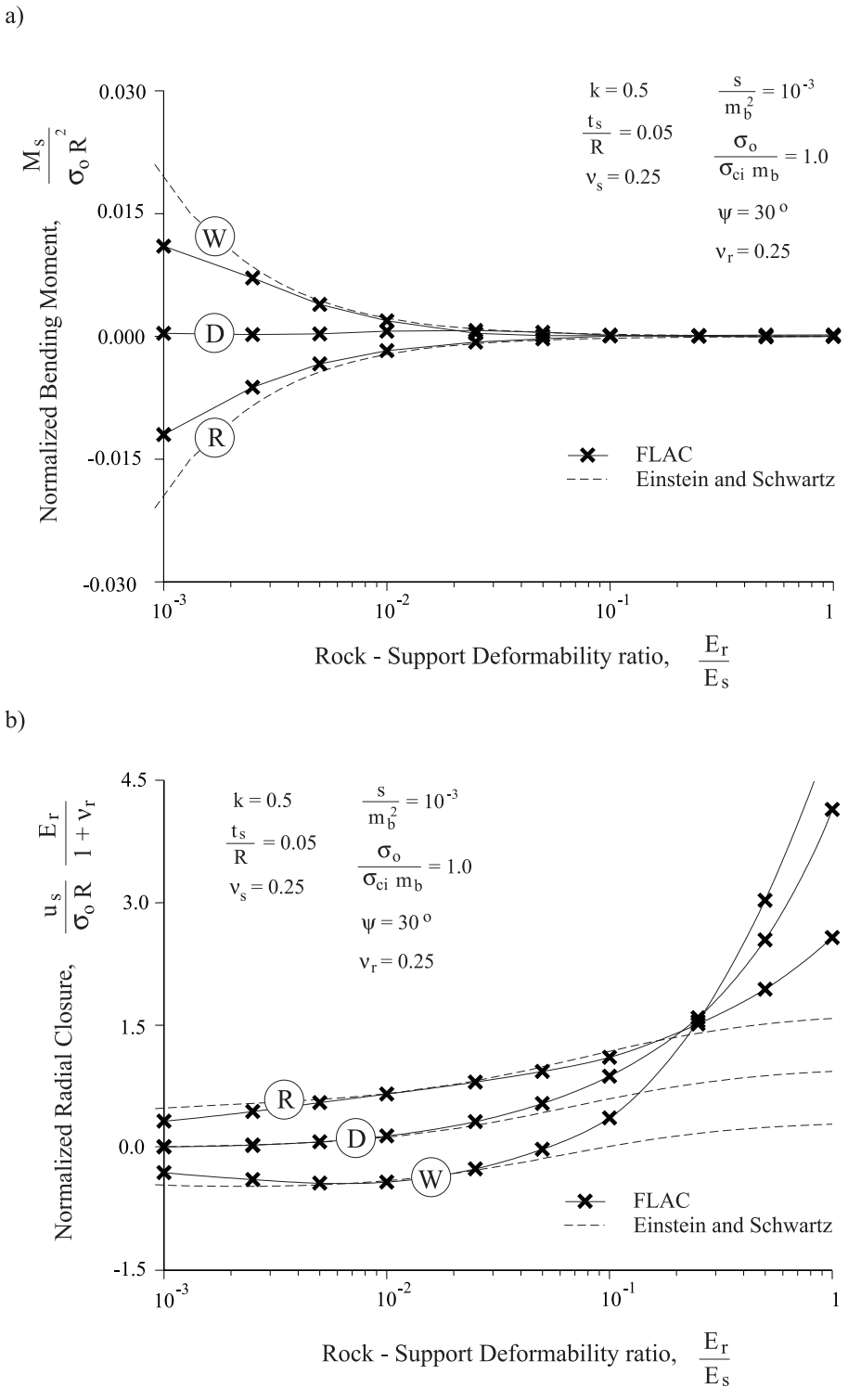

Figure 14. Comparison of a) bending moment and b) radial displacement of the the lining as obtained with Einstein and Schwartz (1979) elastic solution and with elasto-plastic numerical models.

Note that, from equation (4), the far-field stresses are uniform (or *hydrostatic*) if $k = 1$ and, non-uniform (or *non-hydrostatic*) if $k \neq 1$.

The goal of the analysis is to determine the distribution of thrust T_s, bending moment M_s and radial displacement u_s on a section of support of unit length as a function of the angle θ (see the sketch on the right in Figure 13a) for the cases in which *i)* the rock-mass remains elastic and *ii)* the rock-mass fails (i.e., deforms elasto-plastically).

Considering the symmetry of the problem with respect to horizontal and vertical planes containing the axis of the tunnel, the loads and displacements are recorded at three sections of the support, indicated as 'R', 'D' and 'W' in Figure 13a (corresponding to 'Roof', 'Diagonal' and 'Wall' respectively).

The support is assumed to be connected rigidly to the surface of the rock-mass (i.e., it is assumed that no slip occurs at the rock-support interface). The analysis also considers an 'instant' transfer of loads from the rock-mass to the support. Since this implies that the beneficial effect of the position of the face is not taken into account, the calculated loads on the support are sometimes assumed to be overestimated by this (Einstein and Schwartz) method —see, for example Panet (1995). [The discussion in footnote 8, page 19, on long-term degradation suggests that this overestimate may be less than indicated.]

Figures 13b and 14 show results obtained with FLAC comparing the Einstein and Schwartz elastic predictions with those for the case where inelastic deformation occurred with significant (30°) dilation.

It is seen that, *i)* for cases in which the Rock Mass Rating RMR (Bieniawski 1976) or GSI (Hoek and Brown 1997) characterizes a rock-mass as 'Poor' to 'Very Good' (e.g., values of rock-support deformability ratio E_r/E_s ranging from 10^{-2} to 10 —see Appendix B) the design of tunnel supports based on the assumption of elastic behavior as described by Einstein and Schwartz can lead to significant underestimation of the loads and deformations induced on the support (Figures 13b and 14). *ii)* For rock-masses characterized as 'Very Poor' (e.g., values of rock-support deformability ratio E_r/E_s below 10^{-2}) the Einstein and Schwartz design approach can lead to overestimation of the loads and deformations on the support —i.e., the approach is conservative.

A full discussion of the consequences of inelastic deformation on the Einstein-Schwartz method is given in Carranza-Torres and Fairhurst (2000a).

Convergence-Confinement Design and the New Austrian Tunneling Method

The so-called New Austrian Tunneling Method (NATM) evolved during the 1950's and early 1960's, stimulated by the work of the Austrian civil engineers Rabcewicz, Muller, Pacher, Golser and colleagues involved in driving of transportation tunnels through the Austrian Alps. The NATM differs from the methods discussed above in that the support load required to stabilize the excavation is considered to vary with inward convergence of the tunnel, and is not prescribed in advance; rather the support is varied on site as required to ensure that the excavation is stable. Calculation of the

required support is a statically indeterminate problem, and is assessed by examination of the rock-support interaction as described by *convergence-confinement* curves.

The theoretical basis of convergence-confinement analysis has been described and used in tunnel support design well before the NATM was introduced —e.g., Fenner (1938), Labasse (1949), Talobre (1957), Kastner (1962). The contribution of the NATM was to develop practical tunneling support procedures, based on the convergence-confinement principle, which allowed the support to be optimized on site.

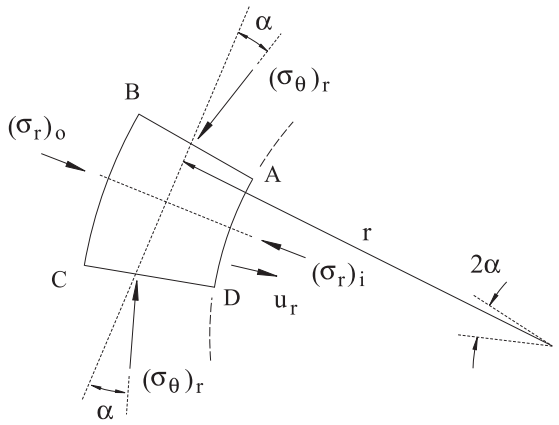

Figure 15. Forces acting on an elementary wedge in the vicinity of an excavation.

The convergence-confinement philosophy can be illustrated by considering the simple case of a circular excavation in a homogeneous rock subject to uniform in situ stress —as in the case of Lamé's solution in Figure 1a. A uniform radial pressure (the support) is applied at the wall of the tunnel. Consider a wedge-shaped element of the rock bounded by two lines radiating from the center of the tunnel and two circumferential lines, in the vicinity of the excavation, as shown in Figure 15. Prior to excavation, each face of the wedge will be subject to the same uniform force acting normal to the face. Excavation of the tunnel will reduce the force acting radially outward on the inner face. The force on the outer face will be reduced also, but less so than on the inner face. The unbalanced radial force will cause the element to move radially towards the excavation. This will 'tighten the wedge' —i.e., the tangential force acting on the sides of the wedge will increase. A (small) component of the tangential force is directed radially outward, tending to reduce the net inward radial force. The wedge will tighten (i.e., displace towards the center of the tunnel), and the tangential stress will increase correspondingly until the wedge comes to equilibrium with the radial (support) pressure on the wall of the excavation. If the support pressure is reduced, the wedge will displace further towards the tunnel until the forces are again in equilibrium. As long as the tangential stress continues to increase as the wedge

displaces radially inwards, then the tunnel will find an equilibrium position as the support pressure is decreased. Note that this may be true whether the rock deforms elastically or inelastically. A lower rate of tangential stress increase with deformation simply implies that the radial displacement (convergence) will be greater before an equilibrium condition is reached. In some cases the tangential stress may reach an upper limit beyond which the wedge may 'fail'. This may cause various results such as pore collapse in the case of a porous rock —e.g., reaching the shear strength of the material, slip along a joint traversing the wedge, etc. In such cases, the support pressure must be increased if stability of the excavation is to be maintained.

[Readers familiar with continuum mechanics will be aware that the above (lengthy) description can be summarized in a single line by the equation of radial equilibrium, used, for example, to derive the Lamé solution for an elastic medium (see Figure 1a).]

Figure 16a shows the typical form of the convergence–confinement diagram, which is usually derived for the case of a circular tunnel in homogeneous isotropic rock under uniform insitu stress [p_o]. Curve *PB*, often referred to as the Ground Reaction Curve, or GRC, indicates the radial deformation [u_r] that would develop when the tunnel came to equilibrium with a radial support pressure [p_i]. The initial segment *PA* indicates elastic deformation; *AB* corresponds to stable inelastic deformation; *BC* indicates the onset of unstable deformation (referred to by Austrian designers as the region of 'loosening pressure'). Kovari (2000) has argued recently that there is no fundamental justification for this loosening regime. It is easily shown, however, that an ascending portion of the curve at larger convergence is entirely possible, especially in the roof of a tunnel if the rock cohesion declines with deformation, and gravitational loads begin to dominate in determining the required support pressure [Daemen (1975)].

The shape and magnitude of the Support Characteristic (SC) —see the three curves indicated as SC in Figure 16a— varies considerably depending on the type of support and the amount of convergence that has occurred prior to support installation. In the simplest case, of a uniform elastic ring installed around the tunnel periphery, the SC is a straight line as determined from the expression for the radial deformation [u_r] of a thin shell loaded externally (i.e., at the rock-support interface) by the radial pressure [p_i].

Figure 16b shows a series of support characteristics for circular steel supports with various spacings of wood blocking between the rock and the steel ring. The characteristic for a thin layer of shotcrete is included for comparison (Daemen 1975). The relatively low stiffness of the steel/wood block combinations arises due to the dominance of the low stiffness of the wood blocking in determining the overall Support Characteristic. Hoek and Brown (1980) discuss the procedure to estimate the stiffness. Although the intrinsic stiffness of the shotcrete is much lower than that of the steel, the fact that it is applied directly to the rock, (i.e., with no intervening blocking) results in a stiffer overall support.

Figure 17 shows a series of Ground Reaction Curves [Daemen (1975); Fairhurst

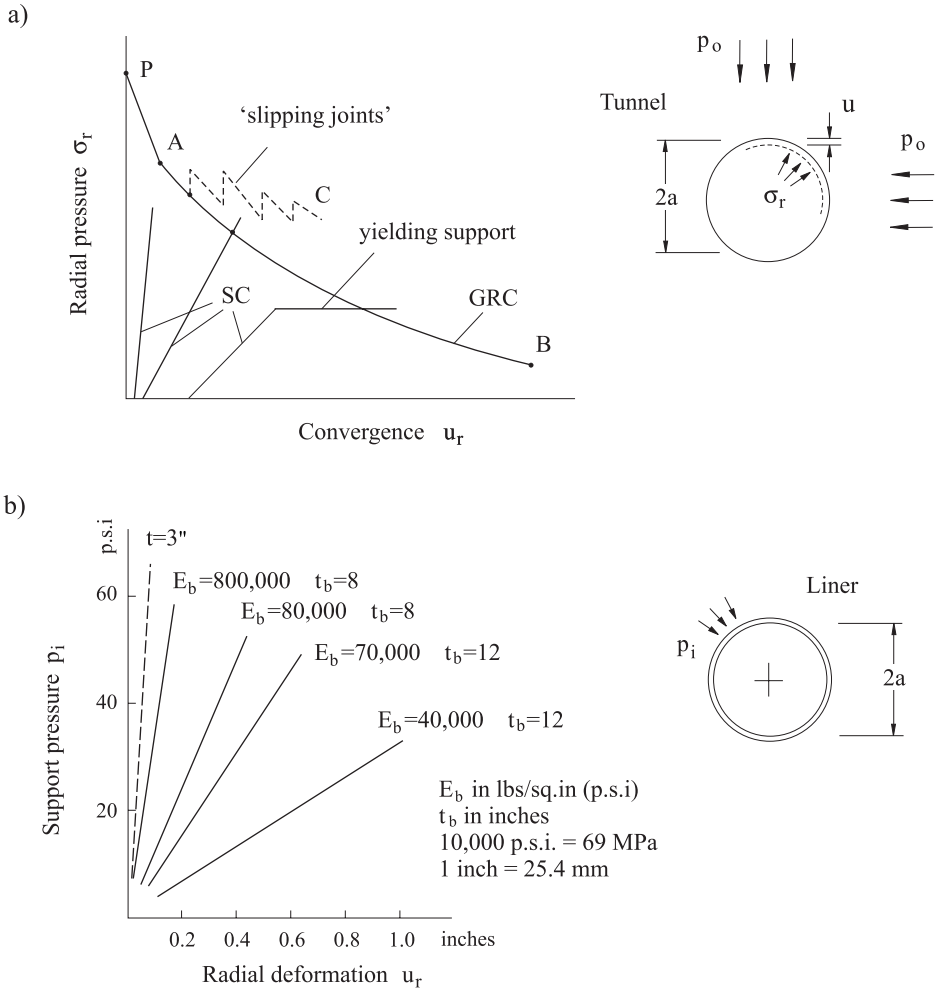

The solid lines are for a wood-blocked steel support for various blocking conditions. The dotted line is the support characteristic for a 3 in. (7.6. cm) thick layer of shotcrete - Modulus E = 3 x 10^6 psi (21,000 MPa).

Tunnel diameter = 16.7 ft (5 m), steel support 6 in (15 cm) x 4 in (10 cm) light beam, 16 lbs/ft (23.6 kg/m), 2 ft (61 cm) spacing. Wood-block spacing = 41.9 in (1.05 m), E_b = block modulus (psi), t_b = block thickness (in). Note how much stiffer the shotcrete suppport is than the steel-arch wood combinations. (The shotcrete will, in fact, not develop its full elastic properties immediately, as assumed here, hence will have lower stiffness at early times.)

Figure 16. a) Interaction between ground reaction curve (GRC) and support characteristic (SC) around underground excavations. b) Support characteristics for various support systems.

Equations used in the construction of the Ground Reaction Curves (after Fairhurst, 1991)

$$p_i = [p_o(1-\sin\phi_i) - c_i\cos\phi_i + c_r\cot\phi_r] \times \left(\frac{a}{b}\right)^{\alpha} - c_r\cot\phi_r$$

where $\alpha = \dfrac{2\sin\phi_r}{1-\sin\phi_r}$

$$\left(u_r^i\right)_{r=a} = \frac{1+\nu}{E}\left(\frac{b^2}{a}\right)[p_o\sin\phi_i + c_i\cos\phi_i] + \left[\frac{(b^2-a^2)(K-1)}{2a}\right]$$

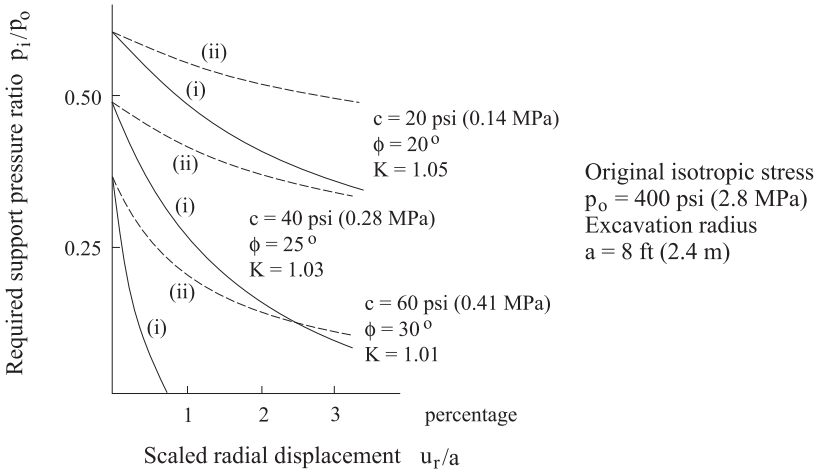

The solid lines (i) indicate the curves for the condition where the rock strength is assumed to be represented by a single Mohr envelope (i.e., $\phi_i = \phi_r$; $c_i = c_r$). The dotted lines (ii) represent cases where the rock strength drops progressively with deformation from the same initial values to the lower residual values ($\phi_i > \phi_r$; $c_i > c_r$).

In the diagram (and equations) above, K is a constant used to express in approximate form the dilation of the plastic zone. Thus K=1.01 implies 1% average (constant) dilation in the plastic region; K=1.05 implies 5% dilation. These values were based on field measurements in sandstones and shales (in coal mines) by Labasse.

Figure 17. Typical support pressure [p_i] versus radial displacement [u_r] curves derived from elasto-plastic models.

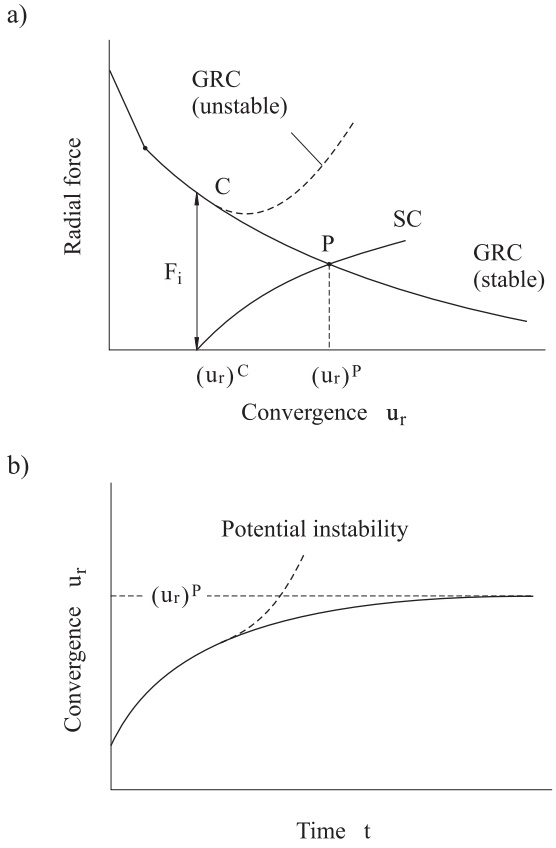

Figure 18. Ground reaction curves as the basis for observation and assessment of the stability of a tunnel.

(1991)] calculated for circular excavations in several hypothetical rock types under uniform loading conditions. Two conditions are shown: *(i)* where the rock cohesion is constant, independent of deformation; and *(ii)* where the cohesion decreases linearly with deformation beyond the peak strength of the rock to a residual cohesion. It is seen that the support pressure required for equilibrium can increase considerably where cohesion decreases; or, equivalently, the amount of convergence may increase considerably if the support pressure is small. Loss of cohesion with inelastic deformation can be gradual in softer rocks (clays and some sedimentary species) or abrupt in more brittle rocks. It is also clear that, if the cohesion of the rock decreases to zero (this will occur first at the tunnel periphery), then the tunnel will inevitably collapse[9].

[9] Consider a small annulus Δr around the tunnel periphery where the cohesion has declined to zero (see, for example, Figure 15). In a cohesionless material, the tangential stress will be proportional to the radial stress. If the radial stress is zero —i.e., the tunnel is unsupported— then the tangential stress will also be zero. This annulus carries no load. It corresponds, in effect, to an enlargement of the tunnel. Since the tunnel is in an infinite medium, the stress distribution around the tunnel, now of radius, $r + \Delta r$, will be the same as for the tunnel radius r. A new annulus will fail-and the process is

Consider the GRC and SC represented in Figure 18a. The support starts to absorve load (i.e., it is installed in place) when the element of tunnel at the periphery has undergone a radial deformation, $(u_r)^C$. The rate at which the convergence will increase will be proportional to the difference in pressure (force) between the GRC and the SC. This rate will decline as the equilibrium convergence is approached. In the case of an inadequate support (the case of the 'unstable' GRC in Figure 18a), the rate will tend to increase beyond the minimum of the GRC. Regular monitoring of convergence rates will thus allow the engineer to assess the adequacy of the support on site, even though the actual magnitudes of the GRC and SC may not be known!

If a condition of impending instability is detected (Figure 18b), then additional support, such as an additional layer of shotcrete, can be applied to 'stiffen' (i.e., increase the slope of) the SC, in order to achieve stability. Thus, successful application of the convergence-confinement method implies a support system that is capable of adapting quickly to rock conditions as they are revealed at the tunnel face, awareness of the importance of maintaining the integrity of the tunnel periphery, and regular monitoring of the convergence rate to ensure that stability is assured —either permanently or, in poor conditions, long enough to allow the installation of more robust permanent support. Although loads on the supports are estimated to guide in the selection of the support system, on site control of deformation (convergence) is the focal point of the method.

Another application of the convergence-confinement method to the assessment of tunnel stability conditions is presented by Hoek in his recent Terzaghi lecture [Hoek (2001)]. Figure 19 —reproduced from the article— shows a classification of the degree of difficulty associated with tunnelling through difficult ground conditions constructed, effectively, in terms of ground reaction curves. An interesting aspect of this classification is that 'squeezing problems' for tunnels are predicted in terms of dimensionless groups of variables (the ratio of far-field stress and strength of the rock and a dimensionless measure of the closure of the tunnel —i.e., the ratio of wall convergence and tunnel radius, referred to as the *strain*).

The construction of the ground reaction curves in Figures 16 through 18 requires the consideration of a 'failure' model for the material. In particular, the ground reaction curves of Figure 17 assume a linear Mohr-Coulomb failure criterion like the one represented in Figure 20a.

Non-linear models describing the failure of the rock are commonly used in tunnel engineering practice. Among them, the Hoek-Brown failure criterion is

---

repeated without limit —i.e., the tunnel collapses totally. If, however, the annulus around the original tunnel retains some cohesion, albeit small, then a tangential stress will develop and the tunnel will be stable (although in some cases the convergence may be more than is acceptable). This illustrates the importance of maintaining some integrity of the tunnel wall. This is especially true when rock bolts are the primary support. Special attention must be paid to prevention of fallout and 'unraveling' (e.g., by use of wire mesh between the bolts) especially in broken rock, prior to placing of additional support such as shotcrete.

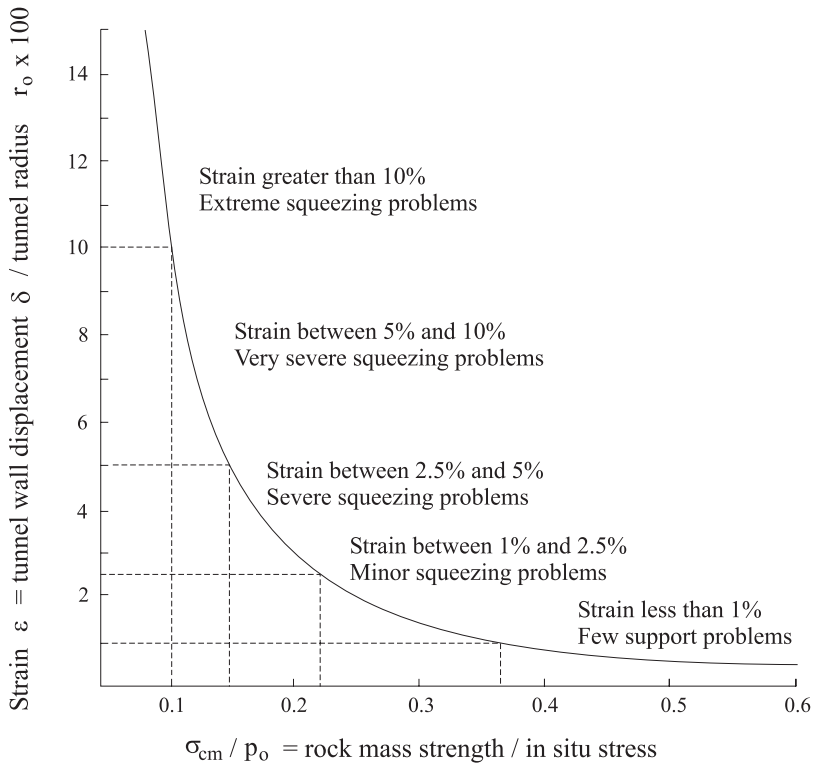

Figure 19. Tunnelling problems associated with different levels of strain (after Hoek, 2001).

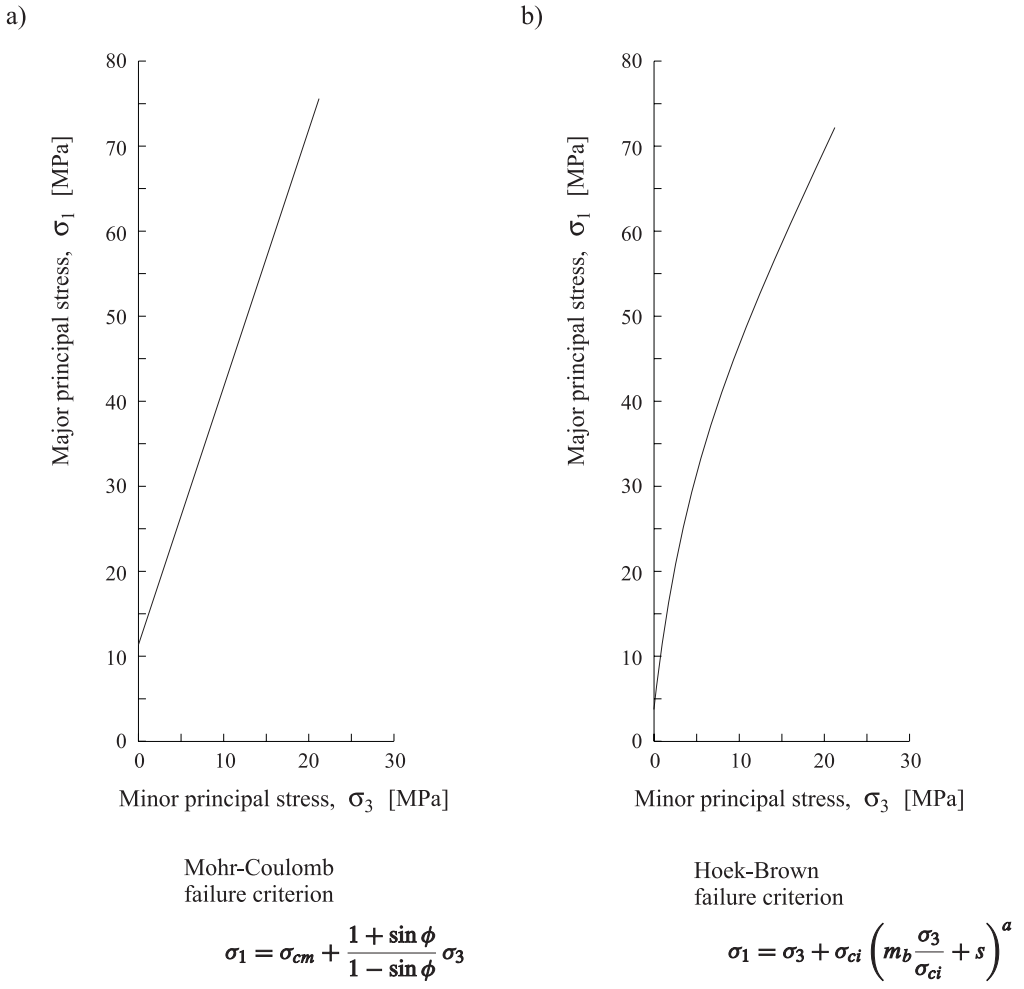

Figure 20. a) Linear Mohr-Coulomb and b) Non-linear (parabolic) Hoek-Brown failure criteria.

the most widely known. Figure 20b represents the parabolic relationship between principal stresses defined by this criterion. The fundamental parameters describing the strength of rock are the unconfined compression strength σ_{ci} of the intact rock, and the parameters m_b, s and a. [Appendix B presents a detailed discussion on the Hoek-Brown failure criterion.]

Construction of the ground reaction curves for rock masses that satify the Hoek-Brown failure criterion can be conveniently simplified by application of a dimensionless transformation proposed by Londe (1988) (see Appendix B).

A dimensionless solution for the construction of the ground reaction curves using Londe's transformation has been presented in Carranza-Torres and Fairhurst (1999). The solution will be briefly discussed here together with a practical example.

Consider the section of a cylindrical tunnel of radius R subject to uniform far-field stress σ_o and internal pressure p_i shown in Figure 21a. The rock mass is assumed to satisfy the Hoek-Brown failure criterion represented in Figure 20b.

The uniform internal pressure p_i and far-field stress σ_o are scaled according to Londe's transformation (equation B-8), to give the scaled internal pressure P_i and the scaled far-field stress S_o respectively,

$$P_i = \frac{p_i}{m_b \sigma_{ci}} + \frac{s}{m_b^2} \tag{5}$$

$$S_o = \frac{\sigma_o}{m_b \sigma_{ci}} + \frac{s}{m_b^2} \tag{6}$$

The pressure p_i^{cr} marks the transition from elastic to plastic behavior of the rock mass —i.e., for an internal pressure $p_i > p_i^{cr}$ the rock remains elastic, and for $p_i < p_i^{cr}$ a plastic region of radius R_{pl} develops around the tunnel. [Note that the pressure p_i^{cr} defines the point A in the GRC of Figure 16a.]

The transformed critical (internal) pressure P_i^{cr} for which the elastic limit is achieved is given by the following expression,

$$P_i^{cr} = \frac{1}{16}\left[1 - \sqrt{1 + 16 S_o}\right]^2 \tag{7}$$

The actual (i.e., non-scaled) critical pressure is found from the inverse of equation (5), i.e.,

$$p_i^{cr} = \left[P_i^{cr} - \frac{s}{m_b^2}\right] m_b \sigma_{ci} \tag{8}$$

Provided $p_i > p_i^{cr}$, the relationship between wall displacement u_r^{wall} and the internal pressure p_i in the *elastic* part of the GRC (i.e., segment *AP* in Figure 16a) is given by the equation,

$$u_r^{wall} = \frac{\sigma_o - p_i}{2G_{rm}} R \tag{9}$$

where G_{rm} is the shear modulus of the rock-mass defined by equation (B-10).

For values of internal pressure $p_i < p_i^{cr}$, the extent of the plastic region R_{pl}

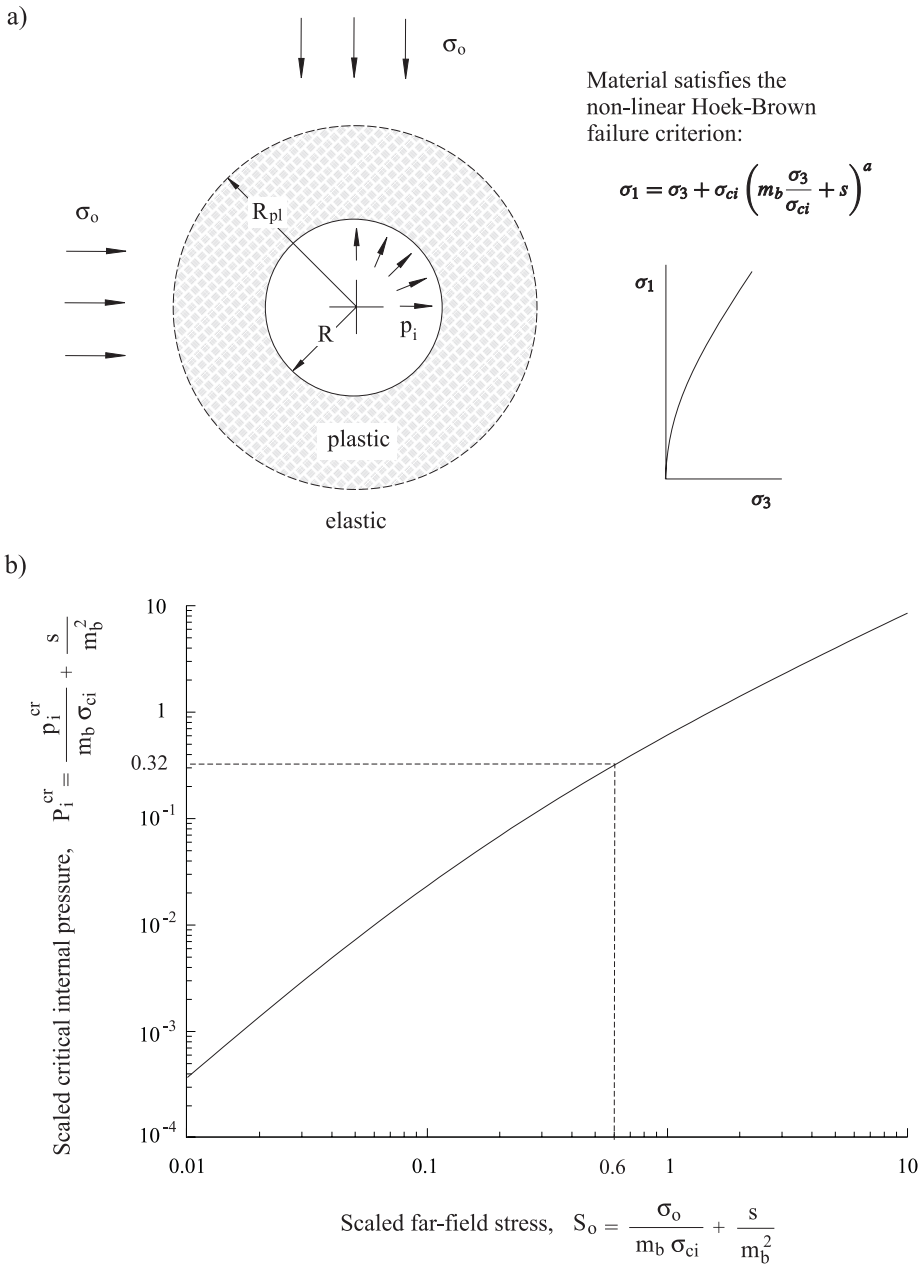

Figure 21. a) Tunnel excavated in a Hoek-Brown material. b) Scaled critical pressure P_i^{cr} as a function of the scaled far-field stress S_o —the critical pressure P_i^{cr} corresponds to the pressure for which the plastic region of radius R_{pl} starts to develop around the tunnel.

that develops around the tunnel is

$$R_{pl} = R \exp\left[2\left(\sqrt{P_i^{cr}} - \sqrt{P_i}\right)\right] \tag{10}$$

To define the plastic part of the Ground Reaction Curve (i.e., the curve *AB* in Figure 16a) a flow rule for the material is needed. The flow rule defines the relationship between the strains that produce distortion and those that produce volumetric changes, as plastic deformation occurs in the material —see for example Atkinson (1993). In underground excavation practice, the flow rule is usually assumed to be linear, with the magnitude of volumetric change characterized by a 'dilation' angle ψ, such that, if $\psi = 0°$, the material undergoes no change in volume during plastic deformation; if $\psi > 0°$, the volume increases during plastic deformation.

In the solution described here, the flow rule will be characterized by a dilation coefficient K_ψ, that is computed from the dilation angle, ψ, according to the expression $K_\psi = [1 + \sin\psi] / [1 - \sin\psi]$. [Note, for example, that for $\psi = 0°$ the dilation coefficient is $K_\psi = 1$ and for $\psi = 30°$, the coefficient is $K_\psi = 3$.]

With the flow rule characterized by the dilation coefficient K_ψ, the plastic part of the GRC —i.e., the segment *AB* in Figure 16a, is given by

$$\begin{aligned} \frac{u_r^{wall}}{R}\frac{2G_{rm}}{\sigma_o - p_i^{cr}} &= \frac{K_\psi - 1}{K_\psi + 1} + \frac{2}{K_\psi + 1}\left(\frac{R_{pl}}{R}\right)^{K_\psi + 1} \\ &+ \frac{1 - 2\nu}{4(S_o - P_i^{cr})}\left[\ln\left(\frac{R_{pl}}{R}\right)\right]^2 \\ &- \left[\frac{1 - 2\nu}{K_\psi + 1}\frac{\sqrt{P_i^{cr}}}{S_o - P_i^{cr}} + \frac{1 - \nu}{2}\frac{K_\psi - 1}{\left(K_\psi + 1\right)^2}\frac{1}{S_o - P_i^{cr}}\right] \\ &\times \left[(K_\psi + 1)\ln\left(\frac{R_{pl}}{R}\right) - \left(\frac{R_{pl}}{R}\right)^{K_\psi + 1} + 1\right] \end{aligned} \tag{11}$$

where ν is the Poisson's ratio for the rock mass.
[A full discussion, with derivations, of equations (5) through (11) is contained in Carranza-Torres and Fairhurst (1999). The equations have been presented here without details in order to focus on their use in obtaining ground reaction curves for the Hoek-Brown failure criterion.]

The dimensionless solution presented above can be conveniently summarized in dimensionless charts. For example, Figure 21b defines the transformed critical internal pressure P_i^{cr} as a function of the transformed far-field stress S_o. Figures 22a and 22b define the extent of the failure region and the scaled convergence at the wall in terms of S_o. The use of these dimensionless relationships will be illustrated with the following practical example.

Consider the tunnel of radius $R = 3.82$ m exacavated at a depth of ~ 1200 m in a rock mass of mean unit weight $\gamma = 25$ KN/m^3 (Figure 23a). The far-field stress

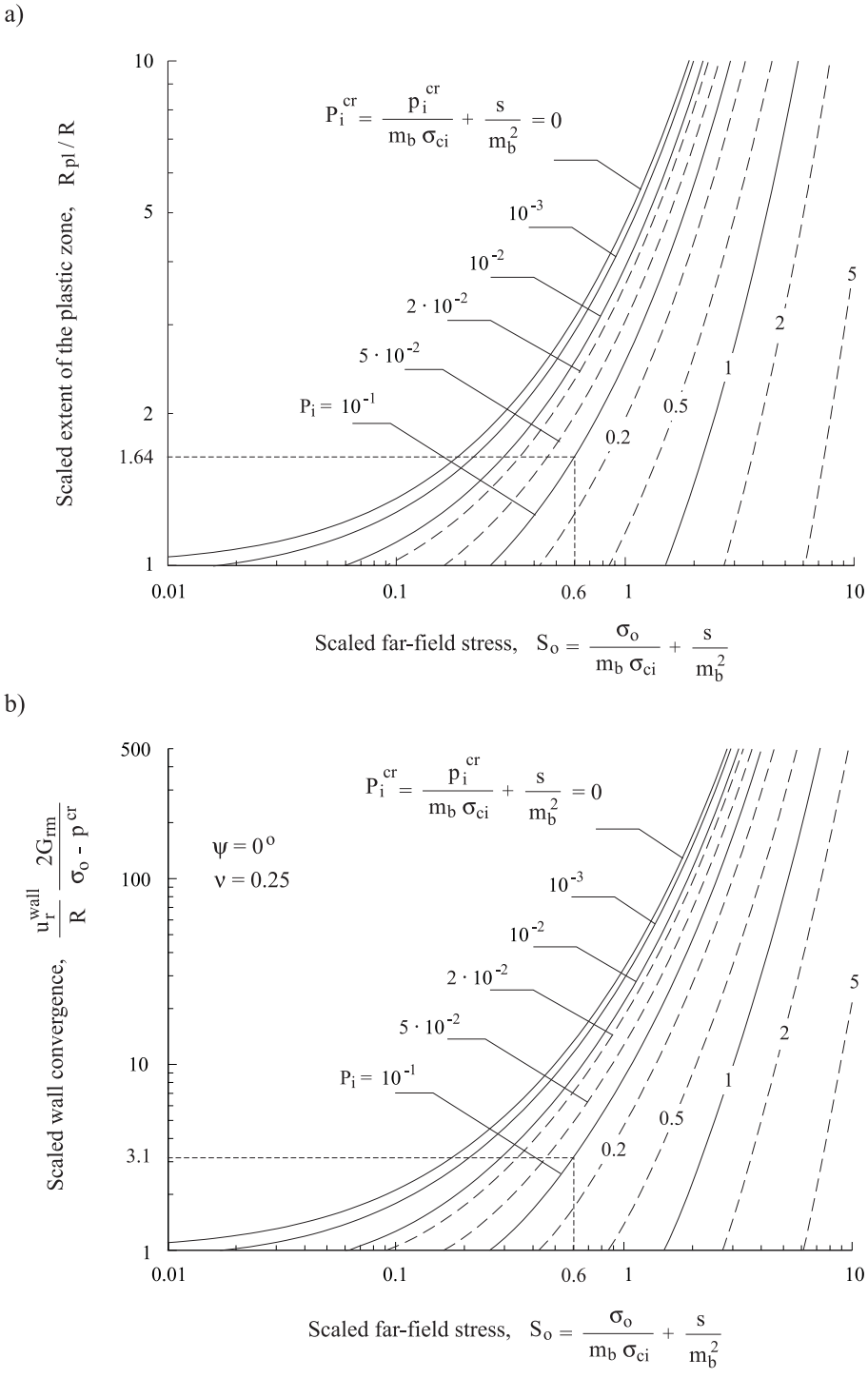

Figure 22. Dimensionless charts for the determination of a) radius R_{pl} of the plastic zone and b) radial convergence u_r^{wall} of wall.

a)

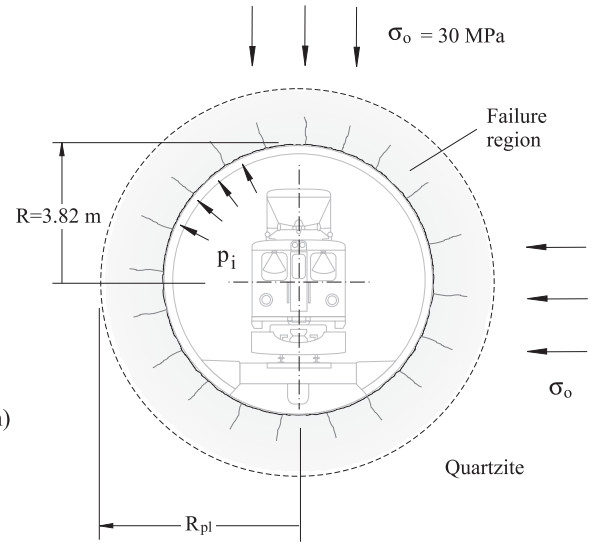

Data

R = 3.82 m

σ_o = 30 MPa
p_i = 5 MPa

σ_{ci} = 30 MPa
m_b = 1.7
$s = 3.9 \cdot 10^{-3}$
a = 0.5

$\psi = 0^o$ (no dilation)

G = 1 GPa
ν = 0.25

b)

Dimensionless values of far-field stress and internal pressure

$$S_o = \frac{\sigma_o}{m_b \sigma_{ci}} + \frac{s}{m_b^2} = 0.6 \qquad P_i = \frac{p_i}{m_b \sigma_{ci}} + \frac{s}{m_b^2} = 0.1$$

a) Critical internal pressure at the elastic limit

From Figure 21b, for $S_o = 0.6$ $\Rightarrow$ $P_i^{cr} = \frac{p_i^{cr}}{m_b \sigma_{ci}} + \frac{s}{m_b^2} = 0.32$ $\therefore$ $p_i^{cr} = 16$ MPa

b) Radius of the plastic zone

From Figure 22a, for $S_o = 0.6$ and $P_i = 0.1$ $\Rightarrow$ $\frac{R_{pl}}{R} = 1.64$ $\therefore$ $R_{pl} = 6.26$ m

c) Wall convergence (for non-dilating material, $\psi = 0^o$)

From Figure 22b, for $S_o = 0.6$ and $P_i = 0.1$ $\Rightarrow$ $\frac{u_r^{wall}}{R} \frac{2G_{rm}}{\sigma_o - p_i^{cr}} = 3.1$

$\therefore$ $u_r^{wall} = 0.08$ m

Figure 23. Example showing of the application of the dimensionless solution for tunnels in Hoek-Brown materials.

at that depth is $\sigma_o = 30$ MPa. We wish to determine the extent of the failure zone R_{pl} and the convergence for a value of internal pressure $p_i = 5$ MPa. The rock mass has been classified in terms of the Hoek-Brown parameters $\sigma_{ci} = 30$ MPa, $m_b = 1.7$, $s = 3.9 \times 10^{-3}$, $a = 0.5$, $\psi = 0°$, $G_{rm} = 1$ GPa and $\nu = 0.25$ (see Figure 23a).

For the given data, the scaled far-field stress and internal pressure are

$$\begin{aligned} S_o &= \frac{\sigma_o}{m_b \sigma_{ci}} + \frac{s}{m_b^2} = 0.6 \\ P_i &= \frac{p_i}{m_b \sigma_{ci}} + \frac{s}{m_b^2} = 0.1 \end{aligned}$$

The scaled critical internal pressure P_i^{cr} at which the elastic limit of the rock mass is reached, can be read from Figure 21b (see equation 7),

$$P_i^{cr} = \frac{1}{16}\left[1 - \sqrt{1 + 16 S_o}\right]^2 = 0.32$$

From this expression, the critical internal pressure p_i^{cr} is found to be $p_i^{cr} =$ 16 MPa. Since the internal pressure for this problem is $p_i = 5$ MPa [< 16 MPa], a plastic region will develop around the tunnel.

The scaled extension R_{pl}/R of failure region can be read from Figure 22a (see equation 10),

$$\frac{R_{pl}}{R} = 1.64$$

Since the tunnel has a radius $R = 3.82$ m, the radius of the failure zone is $R_{pl} = 6.26$ m.

The scaled radial displacement at the wall of the tunnel can be obtained from Figure 22b (see equation 11), and it results to be,

$$\frac{u_r^{wall}}{R} \frac{2G_{rm}}{\sigma_o - p_i^{cr}} = 3.1$$

Replacing the (known) values of the variables on the left side of the expression above, the wall convergence is finally found to be $u_r^{wall} = 0.08$ m.

In the example just discussed, we have considered the particular case of internal pressure $p_i = 5$ MPa. To construct a full ground reaction curve —e.g., the curve *PB* in Figure 16a— the same procedure is applied for decreasing values of p_i, ranging from σ_o to zero. Examples of construction of ground reactions curves for tunnels in Hoek-Brown materials are presented in Carranza-Torres and Fairhurst (2000b).

"Closing the Circle" (1)

The discussion above has emphasized the importance of continuity of the tangential stress around an excavation to ensure stability (see footnote 9 on page 29).

Frequently, in poor quality rock, the excavation may be carried out in sev-

eral stages —e.g., heading and bench or several smaller profiles are excavated and supported separately before being connected to form the final section.

A central rule of NATM, espoused by Rabcewicz and his colleagues was *'close the circle'* as soon as possible. Often this referred to early placement of the invert section of a lining to provide lateral stability to the vertical legs of the support. In all cases, however the message was, in effect, *'ensure continuity of tangential stresses in the rock and/or in the supports around the excavation'.* Loss of this continuity risks the onset of instability. This simple practical guide is entirely consistent with the principles of the Convergence-Confinement method.

Discrete or discontinuum mechanics

The period of 1950 $\sim$ 1960 saw considerable activity worldwide in large-scale civil engineering projects, particularly in dams and hydropower development, and in deep open-pit mining. Stability of large slopes in jointed rock was a prime concern, and classical soil mechanics analyses were not appropriate. The possibilities of using nuclear explosives in major civilian earth-moving projects (e.g., excavation of a new Panama canal) was also under consideration. The mechanics of deformation of assemblages of large discrete blocks was an important concern for these and similar problems.

The growing power of computers suggested that 'tracking' the large number of interactions between individual blocks and the resulting motion and deformation of the block assemblies might be possible. *Discrete* or *discontinuum* codes were developed and discontinuum mechanics is now a vital field of study. Two —and three— dimensional numerical codes such as UDEC (Universal Distinct Element Code) and its three-dimensional counterpart 3DEC [Cundall (1988); Hart, Cundall, and Lemos (1988)] are commercially available and widely used for study of the deformation of blocky and jointed rock. They complement a large number of powerful continuum codes.

Interactions between assemblies of discrete solids are also of considerable significance on the small scale. Computational schemes similar to those for large blocks assemblages can be used, and microparticulate codes such as the Particle Flow Code (PFC), and its three-dimensional counterpart PFC3D [Cundall and Strack (1979); Cundall (1987)], are now providing valuable new insights to problems in rock mechanics where continuum mechanics has been of limited utility.

The 'microparticle' codes assume that forces and deformations are transmitted through the solid via particle to particle interface contacts. Frictional slip and tensions can occur, and cementitious bonding around the contacts can be included. The appropriate properties of the contacts are deduced by calibrating the response of a simulated particulate specimen against laboratory compression tests results.

The power of PFC analysis is well illustrated by the results of simulation of the rock breakout in drifts of the Underground Research Laboratory (URL) of Atomic Energy of Canada Limited at Pinawa, Manitoba, Canada [Cundall (1998); Potyondy

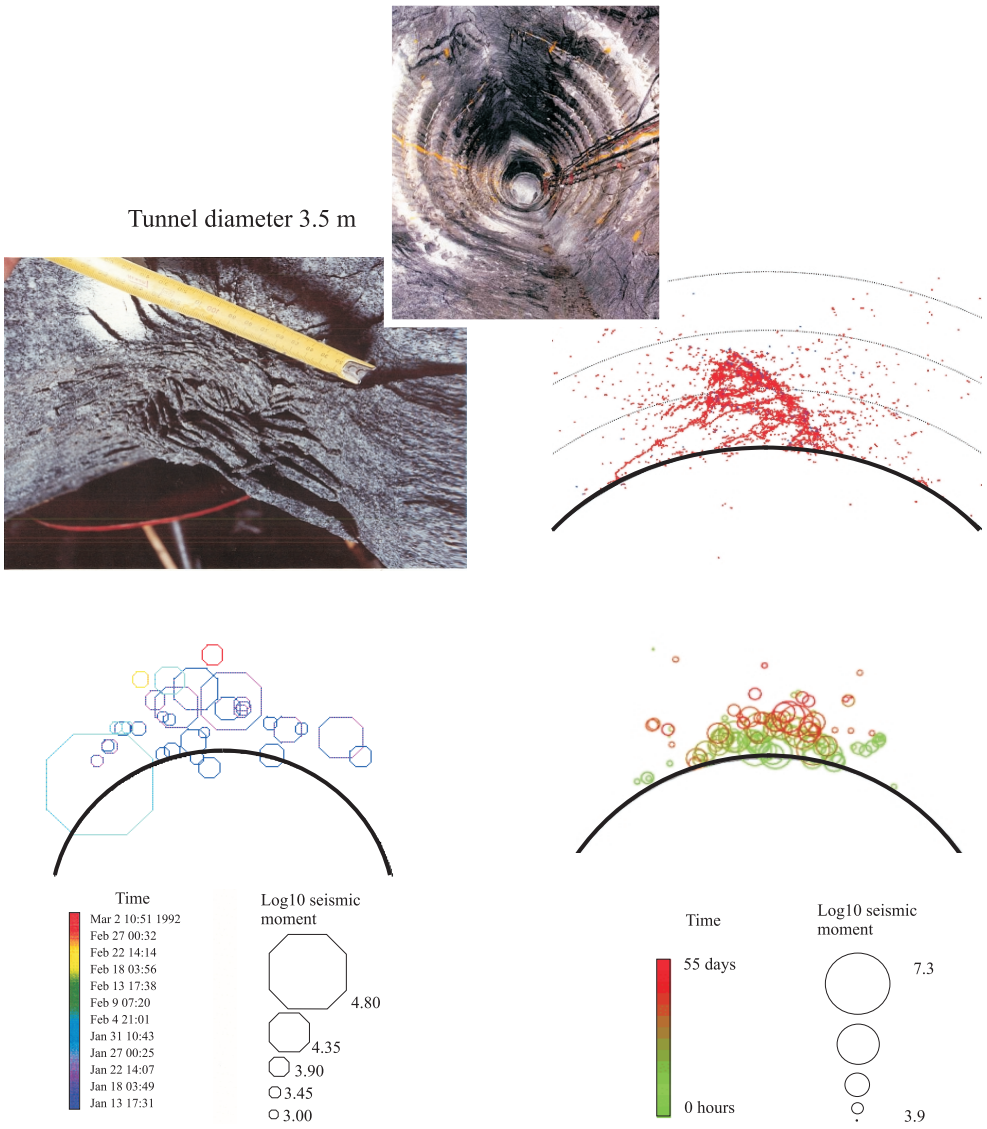

Figure 24. Discrete particle modeling of the Mine-by Tunnel (URL) showing: (top left) view of the mine-by tunnel after excavation; (top right) microcracks that have formed in a very fine resolution PFC2D simulation after 2 months of stress corrosion —i.e., time dependent degradation of rock strength; (bottom left) seismicity recorded during excavation of round 7; (bottom right) seismicity 'recorded' in a coarse resolution PFC2D simulation. (Courtesy of Atomic Energy Canada Ltd.)

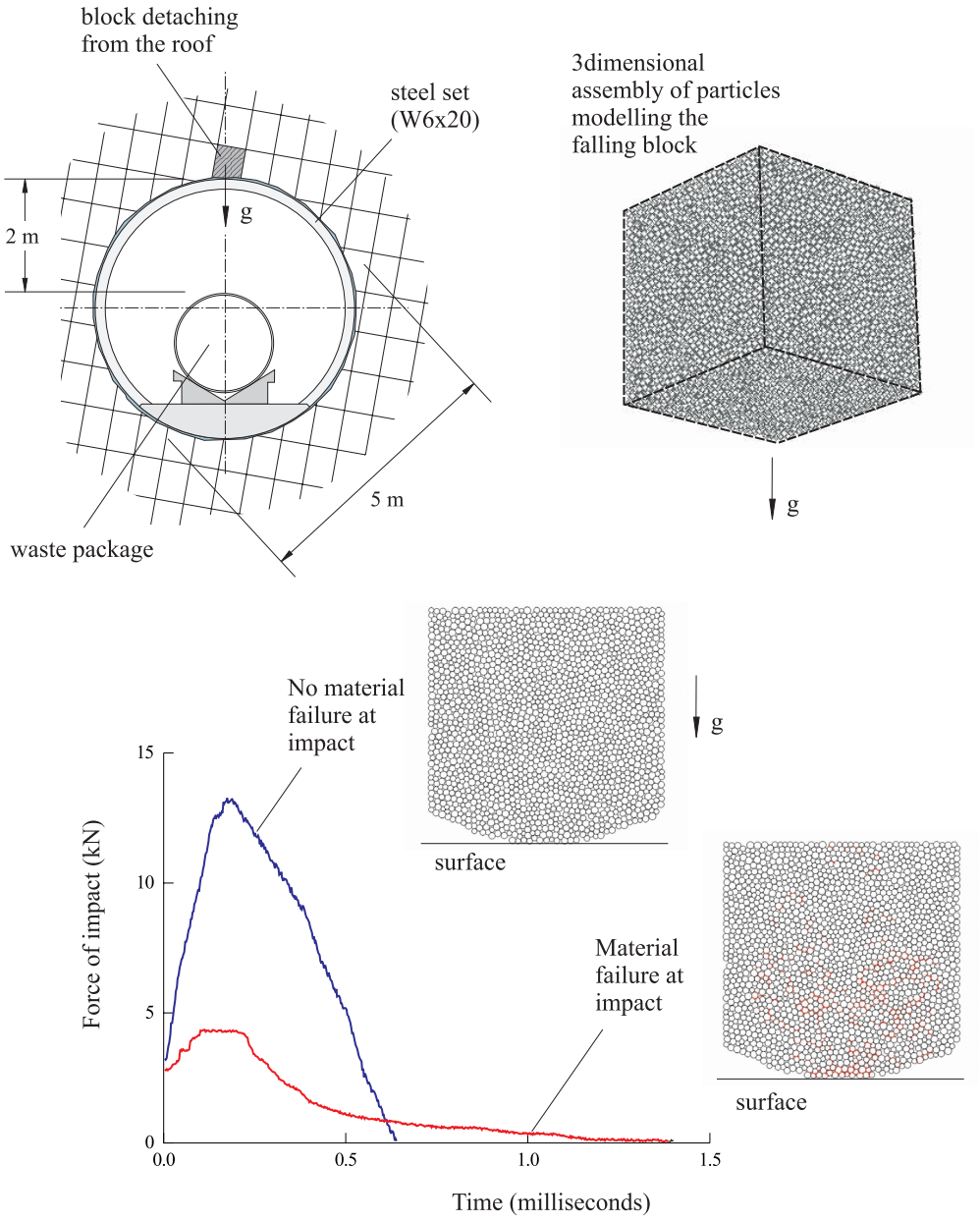

Figure 25. Discrete particle modelling of the impact forces generated by a block of rock that detaches from the roof and falls into a radioactive waste package.

and Cundall (1998)].

The drift is excavated in the Lac du Bonnet granite and used to assess the suitability of granite as a high level nuclear waste repository. Due to the high stress environment, the drift, originally circular, fractured extensively in the roof and floor as seen in the top photographs in Figure 24. Such fracturing is of concern since a fractured region adjacent to the tunnels could provide a high permeability pathway for water to come into contact with the waste. Continuum analyses were unsuccessful in predicting the zone of fracturing accurately, and PFC analyses was introduced. Figure 24 summarizes the results. PFC code is a dynamic code —as are FLAC/FLAC3D and UDEC/3DEC— so that it is possible to compute the microseismic energy released due to breakage of interparticle bonds during the loading process. The lower diagrams in Figure 24 show a comparison between the predicted and observed microseismicity, for the predicted and observed damage zone. The agreement is very encouraging.

Figure 25 shows the result of using PFC to examine the impact forces generated on a nuclear waste canister in an open drift (the design proposed for a repository at Yucca Mountain, Nevada), due to a block of rock falling from the roof [Hart and Fairhurst (2000)]. In the initial PFC model, the rock block was deformable, but could not break. The resulting impulse on the canister is shown in the diagram of Figure 25. The peak force is approximately 14 kN. This is high enough to cause concern that the canister could sustain serious damage. In the second model, the same block consists of an assemblage of particles with bond properties selected to provide the rock modulus and strength properties appropriate to the tuff at Yucca Mountain. In this case the rock breaks upon impact. A significant fraction of the initial momentum of the falling block is 'trapped' in the fragments of broken rock and hence the peak force on the canister is reduced by a factor of almost 4. In this case, the canister is able to withstand the impact without serious damage.

"Closing the Circle" (2)

Apparently, a major obstacle to the extension and application of Newtonian molecular theory of structure of bodies in the 17^{th} century was the impossibility of summing the force interactions between the host of individual pairs of molecules in order to arrive at the overall mechanical behavior of the body. While this cannot be achieved even today, the micro-interactions of significance in rocks occur at a substantially larger scale. Already, valuable insights have been obtained from the numerical code PFC, and further developments are underway. Other groups in various countries are also pursuing similar modelling and experimental studies of particulate mechanics. As can be expected, the computational requirements to carry out studies of large numbers of interacting particles are not trivial, especially if one wishes to solve problems in three dimensions. Efforts are now underway to address this issue.

Continuum mechanics has contributed enormously to the development of rock mechanics, as it has in other branches of science and engineering. The ability to obtain rigorous analytical solutions is an invaluable asset, one that allows confidence

to be placed in the validity of approximate numerical solutions —especially when the latter are shown to be in agreement with the analytical results. Some important applications of rock mechanics involve situations where the continuum hypothesis breaks down, and where disintegration or discontinuum behavior must be dealt with. In some cases it is the dominant concern. The development of discontinuum codes, both for large scale and microparticulate problems, provide us with an additional tool to supplement the continuum approach.

It would seem that the computer and these numerical developments have 'closed the circle' for us in another way —one that the eminent scholars of the 17th and 18th centuries would appreciate greatly. We now have complementary tools that can eliminate gaps, allowing us to explore ranges of material behavior beyond those possible hitherto, and to examine a given problem from 'different directions' to increase confidence in the validity of the results obtained by one technique alone. It is a time of opportunity for rock mechanics.

Challenges

Civil Engineering, with its close relation to public works and service to the public, has traditionally relied more heavily on universities for many of its research and development efforts than other branches of engineering. Universities have also been a focal point for research in mining engineering. Several decades ago there were numerous excellent industrial research laboratories in civil, mining and petroleum engineering both in the U.S and abroad. Most of these have since disappeared or contracted considerably in size. These are the three professions where rock mechanics issues are a primary concern.

Thus, if the discipline is to advance, universities must take the lead in rock mechanics research. A great deal of effort in university research over the past two decades or so has been dedicated to development of numerical modelling procedures. These procedures are now sufficiently mature that we are in a position to begin addressing important gaps in the application of rock mechanics to engineering problems.

As noted earlier in this paper, the Hoek-Brown criterion for predicting rock mass strength is probably the most widely accepted internationally. It is thus salutary to read the following comments on this criterion, extracted from a Letter to the Editor[10], submitted by one of the authors of this criterion, Dr. Evert Hoek:

> *'In writing "Underground Excavations in Rock" almost 15 years ago, Professor E.T. Brown and I developed the Hoek-Brown failure criterion to fill a vacuum which we saw in the process of designing underground excavations. Our approach was entirely empirical and we worked from very limited data of rather poor quality. Our empirical criterion and our*

[10] The letter was published in the News Journal of the International Society for Rock Mechanics, Volume 2, Number 2, 1994.

estimates of the input parameters were offered as a temporary solution to an urgent problem.

In retrospect it is clear that we were naive in believing that our "emergency" criterion would soon be replaced by a set of well-researched predictive tools which were adequately substantiated by field studies and back analyses of real rock engineering case histories. In fact the reverse has happened and I am alarmed to see the Hoek-Brown criterion being applied to problems which we did not even dream about when we made those desperate estimates 15 years ago.

The fact that the criterion works, more by good fortune than because of its inherent scientific merits, is no excuse for the current lack of effort or even apparent desire to find a better way. It is my hope that this short note may catch the eye of someone who has the skill and the motivation to pick up the challenge and to lead in the development of better tools for providing us with the input data which we need for rock engineering designs of the future.

Since testing of in-situ rock masses on a realistic scale is not practical, we have only two avenues open to us to remedy this data deficiency. The first is to develop a better understanding of how the component pieces of the rock mass interact to produce the overall behavior which we need to understand in order to use it as input for our analyses. The second is to use back analysis of the observed performance or rock engineering structures to deduce what rock mass properties exist in these structures.'

We now have the analytical and numerical tools to address this problem and others like it. It is not necessary for university researchers to await the arrival of field data. There are several well established empirical 'classification systems' and tabulations, built up over several decades, to allow the design and/or performance of an underground structure to be assessed on the basis of the performance of many 'similar' structures.

We now have the analytical/numerical tools to begin to establish the framework upon which to arrange these data bases into more rational systems. [Fakhimi (1992) took a step in this direction with respect to Lauffer's (1958) Stand-Up Time Classification.]

These new systems will have the added merit of allowing a more reliable extrapolation beyond the 'experience limits' of the current systems. This is especially needed now when so many projects are moving beyond the limits of current experience.

Universities need to respond to Dr. Hoek's message, and to other field scale problems that we are now in a position to address.

Conclusions

1. Analytical and numerical studies indicate that the Terzaghi Rock Load approach to support design is very conservative.

2. Although no numerical studies have been completed to date, it would appear that Lang's design approach is likely to be conservative (see also conclusion 5 below).

3. Numerical analysis indicates that the Einstein–Schwartz design procedure is conservative in higher quality 'good' to 'very good' rock masses, but can be non-conservative in 'poor quality' rock. It seems to be a useful approach to support design if these limitations are recognized and taken into account.

4. The convergence-confinement method of analysis of the interaction between a tunnel support and the rock mass is the most rational procedure and has been adopted in many countries as the standard.

   The method is entirely consistent with the so called *New Austrian Tunnelling Method*. In this method an initial support-system is selected, one that can be readily modified as tunnel closure measurements indicate to be required.

5. Although the function of rock bolts in tunnel support has been examined by numerous investigators, further study is still required to establish the reinforcement mechanisms of grouted bolts in weak rock.

6. Extension of convergence-confinement procedure to the non-uniform loading case provides valuable insights into behavior of supports under realistic (i.e., non-uniform) loading.

7. University geomechanics research groups have a particular opportunity to advance tunnel support design procedures by using analytical and numerical analysis to establish rational foundations for estimating the deformability and strength of rock masses. This will require special attention to the deformation of joints and joint systems. A larger body of empirical data to test these 'foundations' has been gathered under the general title of 'classification systems'.

Acknowledgment

As noted in the Preamble to this paper, tunnel support design has been a subject of research at the University of Minnesota for almost four decades.

This started with a chance meeting between the Senior Author and Kenneth S. Lane, a senior engineer staff member with the U.S. Army Corps of Engineers, Missouri River Division, in 1957 at the Second U.S. Rock Mechanics Symposium in Golden, Colorado. Ken Lane was a prime mover in the development of the first Tunnel Boring Machine (see footnote 3 on page 4) and an indefatigable campaigner for improvements in geotechnical engineering.

It was Ken Lane who proposed the topic, Rational Design of Tunnel Supports, feeling that U.S. tunnel support design procedures at that time could be improved. The research project Rational Design of Tunnel Supports was started under the sponsorship of the Missouri River Division. This project supported the thesis research of several Ph.D students, including Jaak J.K. Daemen (1975), Michael D. Voegele (1978) and Emmanuel Detournay (1983).

Dr. Peter A. Cundall, then a post-doctoral Research Associate, submitted a research proposal to the National Science Foundation for research to develop an early version of his discontinuum code. The proposal was declined, a decision influenced apparently by a reviewer's opinion that the proposal goal was overly ambitious and unlikely to succeed. Ken Lane and his colleagues recognized the potential of the research and were able to provide sufficient funding to carry forward Dr. Cundall's work. The results were presented as a Corps of Engineers Report in 1974 [Cundall (1974)]. This initial stimulus led to the development of the discontinuum code UDEC, now used internationally for analysis of deformations in blocky and jointed rock. Drs. Don Banks and Jim Drake of the Waterways Experiment Station U.S. Army Corps of Engineers Vicksburg, Mississippi, were also strong supporters.

It is a privilege for the senior author to have been associated with these engineers and many others, including students and faculty, an exceptional group —including my co-author— from whom much has been learned over the past (almost) fifty years.

We hope that this review, albeit personal, will be of interest to participants in this 50th Minnesota Conference on Geotechnical Engineering.

References

American Society of Civil Engineering (1984). *Guidelines for tunnel lining design*. Edited by T. D. O'Rourke. ASCE Technical Council on Research. Technical Committee on Tunnel Lining Design.

Atkinson, J. (1993). *An Introduction to the Mechanics of Soils and Foundations*. Mc Graw–Hill Book Company.

Barton, N., R. Lien, and J. Lunde (1974). Engineering classification of rock masses for the design of tunnel support. *Rock Mechanics and Rock Engineering 6*(4), 189–236.

Bieniawski, Z. T. (1976). Rock mass classification in rock engineering. In Z. T. Bieniawski (Ed.), *Proc. of the Symp. in Exploration for Rock Engineering. Cape Town*, pp. 97–106. Balkema.

Caquot, A. and J. Kerisel (1956). *Traité de Mécanique des Sols*. Paris: Gauthier-Villars.

Carranza-Torres, C. (1998). *Self-Similarity Analysis of the Elasto-Plastic Response of Underground Openings in Rock and Effects of Practical Variables*. Ph. D. thesis, University of Minnesota.

Carranza-Torres, C. and C. Fairhurst (1999). The elasto-plastic response of underground excavations in rock masses that satisfy the Hoek-Brown failure criterion. *International Journal of Rock Mechanics and Mining Sciences 36*(6), 777–809.

Carranza-Torres, C. and C. Fairhurst (2000b). Application of the convergence-confinement method of tunnel design to rock-masses that satisfy the Hoek-Brown failure criterion. *Tunnelling and Underground Space Technology*, 187–213. Vol. 15, No. 2. Pergamon.

Carranza-Torres, C. and C. Fairhurst (2000a). Some consequences of inelastic rock mass deformation on the tunnel support loads predicted by the Einstein and Schwartz approach. In J. F. Labuz, S. D. Glaser, and E. Dawson (Eds.), *Trends in Rock Mechanics. Geo Institute. American Society of Civil Engineers*, pp. 16–49.

Caw, J. M. (1956). The Kolar Gold Field. *Mine and Quarry Engineering 22*, 306–316. London.

Coker, E. G. and L. N. G. Filon (1931). *A Treatise on Photoelasticity*. Cambridge University Press.

Coulomb, C. A. (1776). *Essai sur une application des régles de maximus et minimus à quelques problémes de statique relatifs à l'architecture*. Memoires de mathématique et de physique. L'Académie Royale des Sciences. Paris.

Cundall, P. (1974). Rational design of tunnel supports: A computer model for rock mass behavior using interactive graphics for the input and output of geometrical data. Technical report, U.S. Army Corps of Engineers. Missouri River Division.

Cundall, P. (1987). Distinct element models of rock and soil structure. In E.T. Brown (Ed.), *Analytical and Computational Methods in Engineering Rock Mechanics*, pp. 164–202. Allen & Unwin. London.

Cundall, P. (1988). Formulation of Three-Dimensional Distinct Element Model —Part 1: A Scheme to Detect and Represent Contacts in a System Composed of Many Polyhedral Blocks. *Int. J. Rock Mech. Min. Sci. & Geomech. Abstr. 25*, 107–116.

Cundall, P. (1998). Rock Stability and Long-Term Damage Assessment in the Mine-by Tunnel at URL, Canada. In *Proceedings of the International Workshop on Reversibility: Scientific and Technical Bases for the Reversibility of Geological Disposal. Paris, November 1998*. 2nd Session. Paper No. 1. Chatenay-Malabry, France: ANDRA, 1998.

Cundall, P. and O. Strack (1979). A discrete numerical model for granular assemblies. *Geotechnique 29*, 47–65.

Daemen, J. J. K. (1975). *Tunnel Support Loading Caused by Rock Failure*. Ph. D. thesis, University of Minnesota.

Deere, D. U. (1968). Geological considerations. In K. G. Stagg and O. C. Zienkiewic (Eds.), *Rock Mechanics in Engineering Practice*, pp. 1–20. John Wiley & Sons.

Deere, D. U., R. B. Peck, J. E. Monsees, and B. Schmidt (1969). Design of tunnel and support systems. Technical report, Department of Civil Engineering. University of Illinois. Contract No. 3-0152 from the U.S. Department of Transportation.

d'Escatha, J. and J. Mandel (1974). Stabilité d'une galerie peu profunde en terrain meuble. *Industrie Minérale 6*, 1–9.

d'Escatha, Y. and J. Mandel (1971). Profondeur critique d'eboulement d'un souterrain. *C.R. Acad. Sc. 273*, 470–473.

Detournay, E. (1983). *Two-Dimensional Elastoplastic Analysis of a Long, Cylindrical Cavity under Non-Hydrostatic Loading*. Ph. D. thesis, University of Minnesota.

Einstein, H. H. and C. W. Schwartz (1979). Simplified analysis for tunnel supports. *ASCE J. Geotech. Eng. Div. 105*(4), 449–518.

Fairhurst, C. (1991). General philosophy of support design for underground structures in hard rock. In R. S. Sinha (Ed.), *Underground Structures. Design and Construction*, pp. 1–55. Elsevier.

Fakhimi, A. A. (1992). *The Influence of Time Dependent Deformation of Rock on the Stability of Underground Excavations*. Ph. D. thesis, University of Minnesota.

Fenner, R. (1938). Untersuchungen zur erkenntnis des gebirgsdruckes. *Glückauf 74*, 681–695 and 705–715.

Franklin, J. A. and E. Hoek (1970). Developments in triaxial testing technique. *Rock Mechanics and Rock Engineering 2*, 223–228.

Frocht, M. M. (1941). *Photoelasticity*. John Wiley & Sons, Inc.

Goodman, R. E. (1980). *Introduction to Rock Mechanics*. New York: Wiley and Sons.

Hart, R., P. Cundall, and J. Lemos (1988). Formulation of Three-Dimensional Distinct Element Model —Part 2: Mechanical Calculations for Motion and Interaction of a System Composed of Many Polyhedral Blocks. *Int. J. Rock Mech. Min. Sci. & Geomech. Abstr. 25*, 117–126.

Hart, R. and C. Fairhurst (2000). Application of discontinuum modeling in geotechnical studies for nuclear waste isolation. In S. A. Yufin (Ed.), *Geoecology and Computers*, pp. 15–28. Balkema. Rotterdam.

Heyman, J. (1972). *Coulomb's Memoir on Statics. An Essay in the History of Civil Engineering*. London: Imperial College Press.

Hoek, E. (1983). Strength of jointed rock masses. Rankine Lecture. *Geotechnique 33*(3), 187–223.

Hoek, E. (1994). The challenge of input data for rock engineering. *News Journal of the International Society for Rock Mechanics 2*(2), 4–16.

Hoek, E. (2001). Big Tunnels in Bad Rock. *ASCE J. Geotechnical and Geoenvironmental Engineering 127*(9), 726–740. The Thirty-Six Karl Terzaghi Lecture.

Hoek, E. and E. T. Brown (1980). *Underground Excavations in Rock*. London: The Institute of Mining and Metallurgy.

Hoek, E. and E. T. Brown (1997). Practical estimates of rock mass strength. *Int. J. Rock Mech. Min. Sci. & Geomech. Abstr. 34*(8), 1165–1186.

Hoek, E., P. K. Kaiser, and W. F. Bawden (1995). *Support of Underground Excavations in Hard Rock*. Rotterdam: Balkema.

Inglis, C. E. (1913). Stresses in a plate due to the presence of cracks and sharp corners. *Trans. Instn. Nav. Archit. 55*, 219–241. London.

Isaacson, E. (1958). Rock pressure in mines. *Mining Publications 212*, 31–34. London.

Kastner (1962). *Statik des Tunnel und Stollenbaues*. Springer Verlag.

Kirsch, G. (1898). Die Theorie der Elastizitat und die Bedurinisse der Festigkeitslehre. *V.D.J. 42*(29).

Kooharian, A. (1952). Limit analysis of voissoir (segmental) and concrete arches. *J. American Concrete Inst. 24*(4), 317–328. Dec. 1952.

Kovari, K. (2000). *Personal Communication*. Article submitted to *Felsbau. Rock and Soil Engineering*. Verlag Glückauf GmbH.

Labasse, H. (1949). Les pressions de terrains dans les mines de huiles. *Revue Universelle des Mines*. Liege, Belgium, Series 9, Vol. 5, No. 3, 78-88.

Lama, R. D. and V. S. Vutukuri (1978). *Handbook of Mechanical Properties of Rocks. Testing Techniques and Results*. Volume II. Trans Tech Publications.

Lamé, G. (1852). *Lecǫns sur la théorie de l'elasticité*. Paris: Gauthier-Villars.

Lang, T. A. (1961). Theory and practice of rock bolting. *Trans. Soc. Min. Engrs, Am. Inst. Min. Metall. Petrolm Engrs. 220*, 333–348.

Lang, T. A. (1962). *Notes on Rock Mechanics and Engineering for Rock Construction*. Berkeley. 1962–1964. Volumes I and II.

Lang, T. A. and J. A. Bischoff (1984). Stability of reinforced rock structures. In J. A. Hudson and E. T. Brown (Eds.), *Design and performance of underground excavations*, pp. 11–18. ISRM Symposium–Cambridege, UK.

Lauffer, H. (1958). Gebirgsklassiferung für den Stollenbau. *Geologie und Bauwesen 24*, 46–51.

Londe, P. (1988). Discussion on the determination of the shear stress failure in rock masses. *ASCE J. Geotech. Eng. Div. 114*(3), 374–376.

Marinos, P. and E. Hoek (2000). GSI: A geologically friendly tool for rock mass strength estimation. In *Proceedings of GeoEng2000, An International Conference on Geological and Geotechnical Engineering. November 2000, Melbourne, Australia*.

Muir Wood, A. M. (1975). The circular tunnel in elastic ground. *Geotechnique 25*(1), 115–127.

Obert, L. and W. I. Duvall (1967). *Rock Mechanics and the Design of Structures in Rock*. New York: John Wiley & Sons, Inc.

Panet, M. (1995). *Calcul des Tunnels par la Méthode de Convergence-Confinement*. Press de l'école Nationale des Ponts et Chaussées.

Pippard, A. and R. Ashby (1939a). An experimental study of the voussoir arch. *J. Inst'n. of Civil Engineers 10*. Jan. 1939.

Pippard, A. and R. Ashby (1939b). An experimental study of the voussoir Arch. *J. Inst'n. of Civil Engineers 11–12*.

Pippard, A. and L. Chitty (1941). Repeated load tests on a voussoir arch. *J. Inst'n. of Civil Engineers 17*, 79–86. Nov. 1941.

Potyondy, D. and P. A. Cundall (1998). Modeling Notch-Formation Mechanisms in the URL Mine-by Test Tunnel Using Bonded Assemblies of Circular Particles. In *Proceedings of NARMS'98, 3rd North American Rock Mechanics Symposium*. Paper No. 067. Abstracts included in the Special Issue of the Int. J. Rock Mech. & Min. Sci., 35 (4-5), 1998.

Rabcewicz, L. V. (1964). The New Austrian Tunnelling Method. *Water Power*, 453–515. November 1964.

Ranken, R. E. and J. Ghaboussi (1975). Tunnel design considerations: Analysis of stresses and displacements around advancing tunnels. Technical report, Federal Railroad Administration, United States Department of Transportation. Report No. FRA-ORD 75-84. Washington D.C., Aug. 1975.

Salençon, J. (1969). Contraction quasi-statique d'une cavité á symétrie sphérique ou cylindrique dans un milieu élastoplastique. *Annales des Ponts et Chaussées. IV*, 231–236.

Savin, G. N. (1961). *Stress Concentration Around Holes*. London: Pergamon Press.

Serafim, J. L. and J. P. Pereira (1983). Consideration of the geomechanical classification of Bieniawski. In *Proc. Int. Symp. on Engineering Geology and Underground Construction. Lisbon*, Volume 1(II), pp. 33–44.

Talobre, J. (1957). *La Mécanique des Roches*. Paris: Dunod.

Terzaghi, K. (1943). *Theoretical Soil Mechanics*. John Wiley & Sons, Inc. New York.

Terzaghi, K. (1946). Rock defects and loads on tunnel supports. In R. V. Proctor and T. L. White (Eds.), *Rock tunneling with steel supports*, pp. 17–99. Commercial Shearing and Stamping Company. Youngstown, OH.

Trollope, D. H. (1968). The mechanics of discontinua or clastic mechanics in rock problems. In K. G. Stagg and O. C. Zienkiewic (Eds.), *Rock Mechanics in Engineering Practice*, pp. 275–320. John Wiley & Sons.

U.S. Army Corps fo Engineers (1978). Tunnels and shafts in rock. Technical report, Washington. Dept. of Defense. Dept. of the Army, Corps of Engineers. Gov. Doc. No. D103.6/3:1110-2-2901.

Voegele, M. (1978). *Design of Tunnel Support: An Interactive Based Analysis of the Support Requirements of Excavations in Jointed Rock Masses*. Ph. D. thesis, University of Minnesota.

Voegele, M. and C. Fairhurst (1978). Analysis of tunnel support loads using the distinct block model. In *Storage in Excavated Rock Caverns*, pp. 247–252. Pergamon Press.

Appendix A: Lang's Reinforced Rock Units (RRU's)

a) Definition of variables

The reinforced rock units (RRU) constitute the reinforced zone of the roof of an underground excavation [Lang (1961)]. The factors that contribute to the stability of these units so that they are stable relative to one another and act together as a structural member are (Figure A-1):

- T: Bolt tension
- t: Average bolting stress ($t = T/A$)
- α: Factor depending on time of installation of bolts after excavation (probable variation 0.5 to 1.0)
- γ: Unit weight of the rock
- c: Apparent cohesion of the rock mass (i.e., intrinsic strength at zero normal stress)
- ϕ: Angle of internal friction of the rock mass
- μ: Tangent of the friction angle (i.e., $\mu = \tan\phi$)
- k: Ratio of average horizontal to average vertical stresses
- A: Area of reinforced rock unit (i.e., $A = s^2$ for a bolt pattern with $s \times s$ spacing)

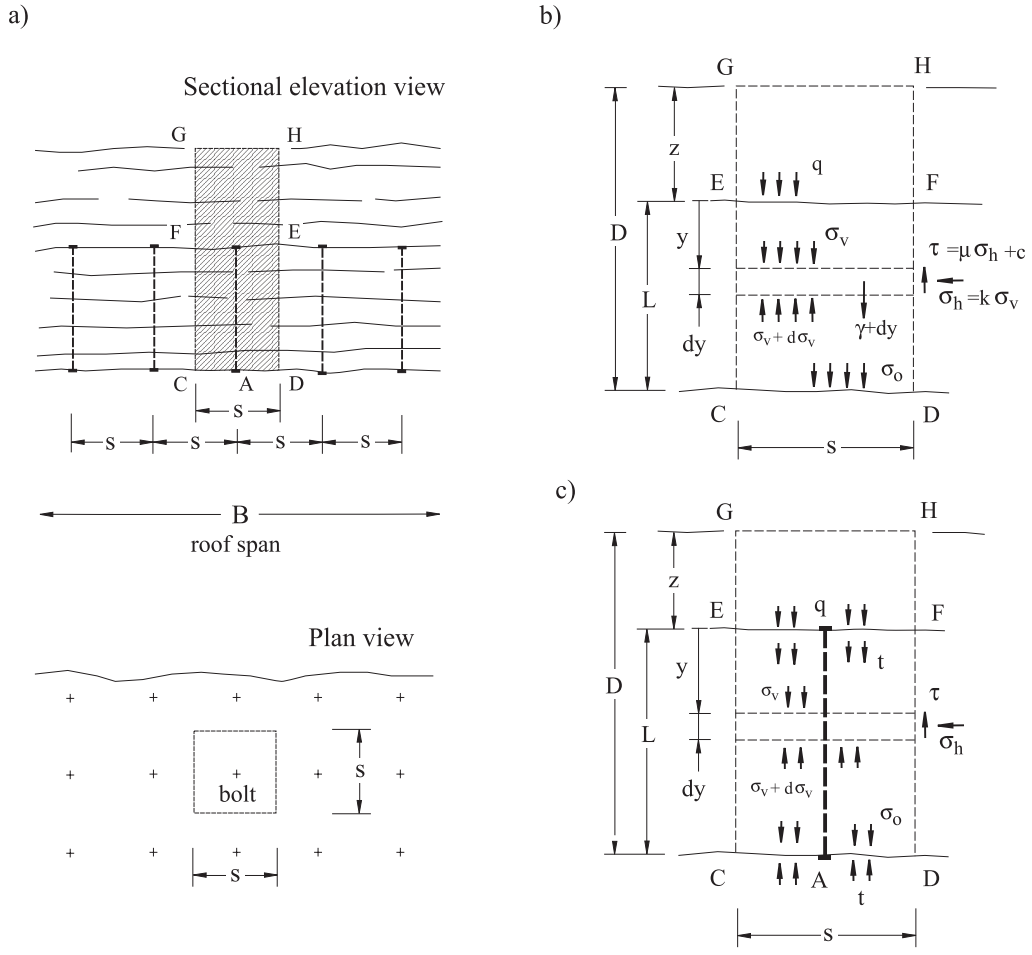

Figure A-1. Rock Reinforced Units (after Lang, 1961).

- P: Shear perimeter of reinforced rock unit (i.e., $P = 4s$ for a bolt pattern with $s \times s$ spacing)
- R: Shear radius (i.e., $R = A/P$ and therefore $R = s/4$ for a bolt pattern with $s \times s$ spacing)
- h: In situ horizontal stress
- L: Length of rock bolts
- D: Height of distressed rock above the surface of the opening

b) Equilibrium analysis of the Rock Unit

We will consider first the stability of the unreinforced rock unit *CDGH*, shown in Figure A-1b, relative to its neighbors.

The stress distribution at limiting equilibrium is given by

$$\sigma_v = \left(\frac{\gamma s}{4} - c\right)\frac{1}{k\mu}\left(1 - e^{-4k\mu y/s}\right) + qe^{-4k\mu y/s} \qquad \text{(A-1)}$$

where:

- σ_v average vertical stress in the unit at a distance y from *EF*
- σ_h horizontal stress conjugate to σ_v (i.e., $\sigma_h = k\sigma_v$, where k is assumed to be constant)
- q average stress superimposed on the top surface, *EF*, of the unit by overlying strata, *EFGH*, or other loading
- τ shear strength at the sides of the unit ($\tau = \sigma_h \tan\phi + c = k\sigma_v\mu + c$)

Equation (A-1) is obtained as follows.

The unreinforced rock unit *CDGH* of dimensions $s \times s \times D$ (Figure A-1b) is assumed to be in a state of limiting equilibrium —i.e., the unit is about to fall under its own weight and shear is fully mobilized along the four vertical sides of the unit.

Consider the equilibrium of forces of the square element, area s^2 and height $\mathrm{d}y$, located at a distance y from the interface *EF* (Figure A-1b).

A normal stress σ_v acts on the upper face and a normal stress $\sigma_v + \mathrm{d}\sigma_v$ acts on the lower face of the element.

Thus, from force equilibrium we have

$$s^2\mathrm{d}\sigma_v = \gamma s^2\mathrm{d}y - 4sc\mathrm{d}y - 4k\mu\sigma_v s\mathrm{d}y$$

or

$$\mathrm{d}\sigma_v = \left[\gamma - \frac{4c}{s} - \frac{4k\mu}{s}\sigma_v\right]\mathrm{d}y$$

or

$$\frac{\mathrm{d}\sigma_v}{\mathrm{d}y} = A - B\sigma_v$$

where

$$A = \left(\gamma - \frac{4c}{s}\right) \quad \text{and} \quad B = \frac{4k\mu}{s}$$

Integrating the differential equation above we obtain

$$\sigma_v = \frac{A}{B} + De^{-By}$$

where D is a constant of integration to be determined from the boundary conditions.

Given that $\sigma_v = q$ when $y = 0$ (Figure A-1b), we find

$$D = q - \frac{A}{B}$$

and therefore

$$\sigma_v = \frac{A}{B}\left(1 - e^{-By}\right) + qe^{-By}$$

Substituting for A and B, we finally obtain the equation (A-1), i.e.,

$$\sigma_v = \left(\frac{\gamma s}{4} - c\right)\frac{1}{k\mu}\left(1 - e^{-4k\mu y/s}\right) + qe^{-4k\mu y/s}$$

For a given value of y, say $y = L$, the vertical stress, σ_o, at *CD* (Figure A-1b), if it was not a free surface, would be

$$\sigma_o = \left(\frac{\gamma s}{4} - c\right)\frac{1}{k\mu}\left(1 - e^{-4k\mu L/s}\right) + qe^{-4k\mu L/s} \tag{A-2}$$

c) Equilibrium analysis of the Reinforced Rock Unit

The basic element of a rock reinforcement system is the reinforced rock unit (RRU), which consists of an individual bolt and the rock immediately surrounding and adjacent to it (Figure A-1c).

Now if the rock *EFGH* above the unit *CDEF* is behaving in a similar manner to that within *CDEF* —i.e., shear is fully developed along its periphery, then q can be expressed as follows

$$q = \left(\frac{\gamma s}{4} - c\right)\frac{1}{k\mu}\left(1 - e^{-4k\mu z/s}\right) \tag{A-3}$$

and substituting this value in equation (A-2) and letting $D = z + L$ gives

$$\sigma_o = \left(\frac{\gamma s}{4} - c\right)\frac{1}{k\mu}\left(1 - e^{-4k\mu D/s}\right) \tag{A-4}$$

or substituting $R = s/4$

$$\sigma_o = (\gamma R - c)\frac{1}{k\mu}\left(1 - e^{-k\mu D/R}\right) \tag{A-5}$$

In effect, $(\gamma R - c)$ is the passive direct support that a prop under the rock unit would have to provide to prevent fallout of the unit relative to the surrounding rock. However, if $(\gamma R - c)$ is zero or negative, then σ_o becomes zero and theoretically, no support is required.

The *Reinforced Rock Unit* theory is based on the assumption that, providing fallout of the rock material has been prevented, the rock unit *CDGH* has deformed to the extent that failure in accordance with Coulomb's criterion is imminent along the sides of the unit.

Note that equation (A-5) is identical to equation (2) in page 13 when $R = B_1$ and $c = 0$ (see Figure 8a).

d) Force carried by the bolts in the Reinforced Rock Unit

If a stabilizing pressure, t, equal to σ_o is provided by a rock bolt installed at the center of the rock unit (see Figure A-1c) then the total tensile load, T, in the rock bolt will be

$$T = ts^2 \tag{A-6}$$

Assuming that the bolt load T is distributed as an average stress over the section of the rock unit and that the effective length of the rock bolt is equal to L, the rock bolt supplies a passive support pressure, t, at *CD* and an equal stress is added at *EF*.

Under these conditions, it can be shown that, for equilibrium of the unit *CDEF*, the passive pressure applied by the bolt at *CD*, t, must equal σ_o. Therefore taking $D = (z + L)$ and $R = s/4$, we have

$$t\left(1 - e^{-k\mu L/R}\right) = \alpha \frac{1}{k\mu}\left(\gamma R - c - h\mu\right)\left(1 - e^{-k\mu D/R}\right) \tag{A-7}$$

or

$$t = tA = \alpha \frac{\gamma AR}{k\mu}\left(1 - \frac{c}{\gamma R} - \frac{h\mu}{\gamma R}\right)\left[\frac{1 - e^{-k\mu D/R}}{1 - e^{-k\mu L/R}}\right] \tag{A-8}$$

In the above equations, it is assumed that the downward deformation of the rock unit has proceeded to the stage where the full shear strength of the rock has been developed on the sides of the unit. In other words, the bolt is applying a passive pressure at point *A*, Figure A-1c, which is just adequate to provide support of that portion of the total weight of distressed rock, D, which is not carried by shear on the sides of the unit. For these conditions, $\alpha = 1$.

If the bolts are installed and tensioned either before or immediately after excavation exposes the surface *CD* in Figure A-1c —i.e., before significant deformation has taken place— then the bolts will apply a pressure at *CD* that 'actively' retards deformation of the unit and 'actively' contributes to its stability. Under these conditions, the bolts are described as providing 'active' reinforcement and it can be shown that $\alpha = 0.5$.

In practice, the time of installation of the bolts will be intermediate between these two extremes and, conservatively, $\alpha = 1.0$ has been used throughout these studies. It may be noted that the use of fully grouted but untensioned rock reinforcement, where the tension in the bolts is developed by the rock deformation, would also be intermediate between the 'active' and 'passive' conditions defined above.

Appendix B: The strength and deformability of rock masses according to the Hoek-Brown failure criterion

The Hoek-Brown criterion has found wide practical application as a method of defining the stress conditions under which a rock-mass will deform inelastically and, if not supported adequately, collapse.

The parameters defining the Hoek-Brown criterion can be estimated from a

combination of laboratory tests on intact rock cores and an empirical 'adjustment' to account for the reduced strength of the rock-mass due to the presence of weaknesses and jointing.

It must be noted that this criterion assumes continuum-isotropic behavior for the rock-mass and should not be applied to cases in which there is a preferred orientation of jointing, such that the mass would not behave as an isotropic continuum.

Testing of rock specimens under triaxial conditions of loading allows the combination of stresses that lead to failure (or collapse) of the specimen to be determined. According to Hoek and Brown, the failure condition of *intact rock* samples is given by the following parabolic law [(Hoek and Brown 1980)],

$$\sigma_1 = \sigma_3 + \sigma_{ci}\sqrt{m_i \frac{\sigma_3}{\sigma_{ci}} + 1} \qquad \text{(B-1)}$$

where

- σ_3 is the confining stress applied to the sample
- σ_1 is the axial stress that produces failure of the sample
- σ_{ci} is the unconfined compression strength of the intact rock
- m_i is a dimensionless parameter, the value of which depends on the type of rock being tested.

In order to characterize the intact rock in terms of equation (B-1), it is necessary to determine the parameters σ_{ci} and m_i. This is done by statistical analysis of strength (σ_1) observed for various values of confining stress (σ_3) in triaxial tests [(Hoek 1983)].

To illustrate the application of equation (B-1) let us consider the triaxial test results shown in Figure B-1 obtained by Franklin and Hoek (1970) for samples of different rock types: *i)* granite, *ii)* quartz dolerite and *iii)* marble (details of the tests can be found in the original paper). The horizontal and vertical axes in the diagram correspond, respectively, to the confining stress σ_3 and the axial stress at failure σ_1 divided by the unconfined compression strength σ_{ci} for each rock type. The dots represent the pairs (σ_3, σ_1) obtained from the triaxial tests. The solid lines are the corresponding failure envelopes defined by equation (B-1) with the parameters σ_{ci} and m_i computed from regression analysis [see Hoek (1983) for details]. It can be seen that, although there is some dispersion in the results, the general trend is for the scattered points to align to the parabolas defined by equation (B-1)[11].

Triaxial testing of rock samples is an expensive procedure and, in most cases, results of the extensive tests needed to determine the parameters σ_{ci} and m_i in the relationship (B-1) are not available. In this case, when information on the unconfined compressive strength is available (e.g., from UCS tests or, indirectly, from point load

[11] The observed dispersion appears to be proportional to the number of specimens tested, with the highest dispersion for the 48 samples of granite and the lowest for the 14 samples of marble —see Franklin and Hoek (1970).

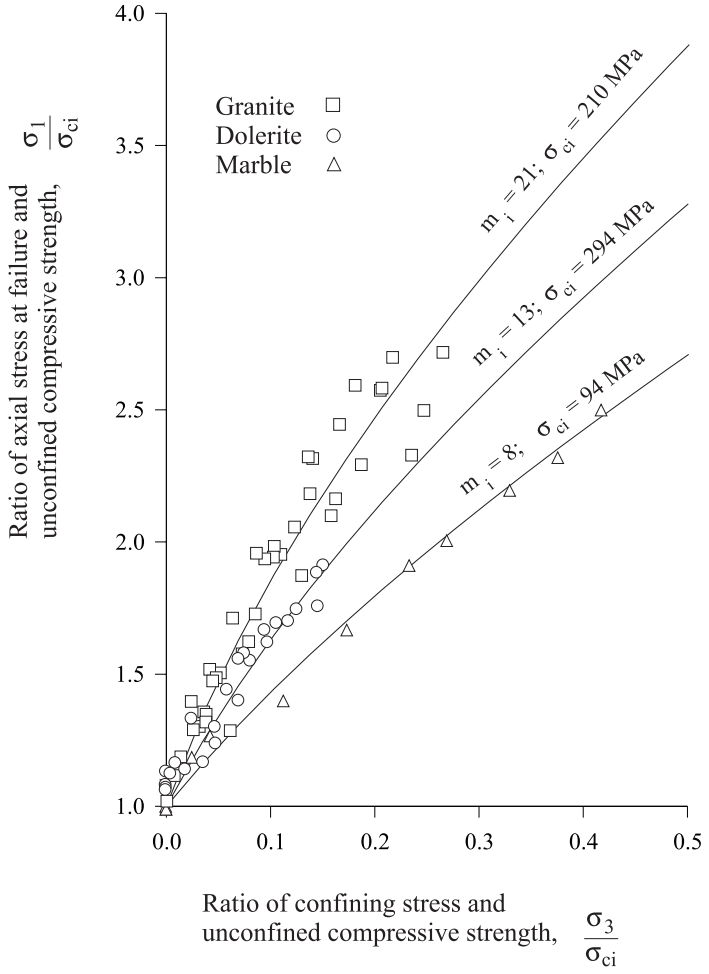

Figure B-1. Failure envelopes obtained from triaxial tests of samples of different rock types (after Franklin and Hoek, 1970). The horizontal and vertical axes represent the confining stress σ_3 and the maximum axial stress σ_1 respectively divided by the unconfined compressive strength σ_{ci} of the sample.

tests), the parameter m_i may be estimated from empirical charts or tables (Hoek et al. 1995).

Table B-1 and Figure B-2, adapted from Lama and Vutukuri (1978), Goodman (1980) and Hoek and Brown (1997) respectively, show typical values of σ_{ci} and m_i for different rock types that could be taken as a reference for use in equation (B-1).

Table B-1. Reference values for the unconfined compressive strength σ_{ci}, Poisson's ratio ν, Young's Modulus E, Shear Modulus G and unit weight γ for intact rock [adapted from Lama and Vutukuri (1978) and Goodman (1980)].

Rock type	σ_{ci} [MPa]	ν	E [MPa]	G [MPa]	γ [MN/m^3]
1) Andesite	130.6	0.16	44.3×10^3	19.1×10^3	25.2×10^{-3}
2) Basalt	148.0	0.32	33.9×10^3	12.8×10^3	27.8×10^{-3}
3) Conglomerate	30.3	0.12	1.3×10^3	0.6×10^3	24.2×10^{-3}
4) Diabase	321.3	0.28	95.8×10^3	37.4×10^3	28.8×10^{-3}
5) Dolomite	46.9	0.29	29.0×10^3	11.2×10^3	24.5×10^{-3}
6) Gneiss	165.0	0.27	76.3×10^3	30.0×10^3	26.8×10^{-3}
7) Granite	141.1	0.22	73.8×10^3	30.3×10^3	26.4×10^{-3}
8) Limestone	51.0	0.29	28.5×10^3	11.1×10^3	23.3×10^{-3}
9) Quartzite	320.1	0.11	88.4×10^3	39.8×10^3	25.7×10^{-3}
10) Sandstone	73.8	0.38	18.3×10^3	6.6×10^3	21.4×10^{-3}
11) Siltstone	122.7	0.22	26.2×10^3	10.7×10^3	25.4×10^{-3}
12) Tuff	11.3	0.19	3.7×10^3	1.5×10^3	23.5×10^{-3}

Origin of the samples: *1)* Palisades Dam, Idaho, USA; *2)* Nevada Test Site, USA; *3)* Mc Dowell Dam, Arizona, USA; *4)* New York, USA; *5)* Minneapolis, Minnesota, USA; *6)* Graminha Dam, Brazil; *7)* Nevada Test Site, USA; *8)* Bedford, Indiana, USA; *9)* Baraboo, Wisconsin, USA; *10)* Amherst, Ohio, USA; *11)* Hackensack, N.Y., USA; *12)* Nevada Test Site, USA.

As noted earlier, joints and defects in a rock-mass reduce the strength of the mass below the strength of an intact specimen of the same rock type. By using the so-called *Geological Strength Index* (or *GSI*) as a scaling parameter, the failure criterion defined by equation (B-1) can be adjusted to provide an estimate of the decreased strength of the rock-mass in the field.

According to Hoek and Brown (1997) the GSI is an empirically derived number that varies over a range between 10 and 100 (the GSI is dimensionless), and can be estimated by examination of the quality of the rock-mass in situ — by direct inspection of an outcrop, for example. By definition, GSI values close to 10 correspond to very poor quality rock-masses, while GSI values close to 100 correspond to excellent quality rock-masses.

Figure B-3 [adapted from Hoek and Brown (1997) and Marinos and Hoek (2000)] shows how the GSI can be estimated from the structure and surface conditions of the rock-mass (for example, a rock-mass with *Blocky/Disturbed* structure and *Poor* surface condition will have a GSI close to 30).

Rock type	Class	Group	Texture		
			Coarse	Medium	Fine
SEDIMENTARY	Clastic		Conglomerate (22)	Sandstone (19)	Siltstone (9)
	Non-clastic	Organic	..... Coal (8~21)		
		Carbonate	Breccia (20)	..... Limestone (8~10)	
METAMORPHIC	Non-foliated		Marble (9)	Hornfels (19)	Quartzite (24)
	Slightly foliated		Migmatite (30)	Amphibolite (25~31)	Mylonites (6)
	Foliated		Gneiss (33)	Schists (4~8)	Phyllites (10)
IGNEOUS	Light		Granite (33)		Rhyolite (16)
			Granodiorite (30)		Dacite (17)
	Dark		Gabbro (27)	Dolerite (19)	Basalt (17)
	Extrusive pyroclastic		Agglomerate (20)	Breccia (18)	Tuff (15)

Figure B-2. Reference values for the coefficient m_i for different rock types (adapted from Hoek and Brown 1997). The value of m_i is shown in parentheses below the name of the rock.

The value $GSI = 25$, indicated by a discontinuous line in Figure B-3, is significant in that it defines the limit between rock-masses of very poor quality ($GSI < 25$) and those of good to reasonable quality ($GSI > 25$). For rock-masses of good to reasonable quality (i.e., $GSI > 25$) the Geological Strength Index is equivalent to the *Rock Mass Rating (RMR)* introduced by Bieniawski (1976) when the rating for *Groundwater* is assessed as 'dry' and the rating for *Joint Orientation* as 'favorable'.

When the scaling factor GSI is introduced, the Hoek-Brown failure criterion for the *rock-mass* is given by the following relationship [Hoek and Brown (1997)]

$$\sigma_1 = \sigma_3 + \sigma_{ci}\left(m_b\frac{\sigma_3}{\sigma_{ci}} + s\right)^a \qquad \text{(B-2)}$$

The parameter m_b in equation (B-2) depends on both the intact rock parameter m_i,

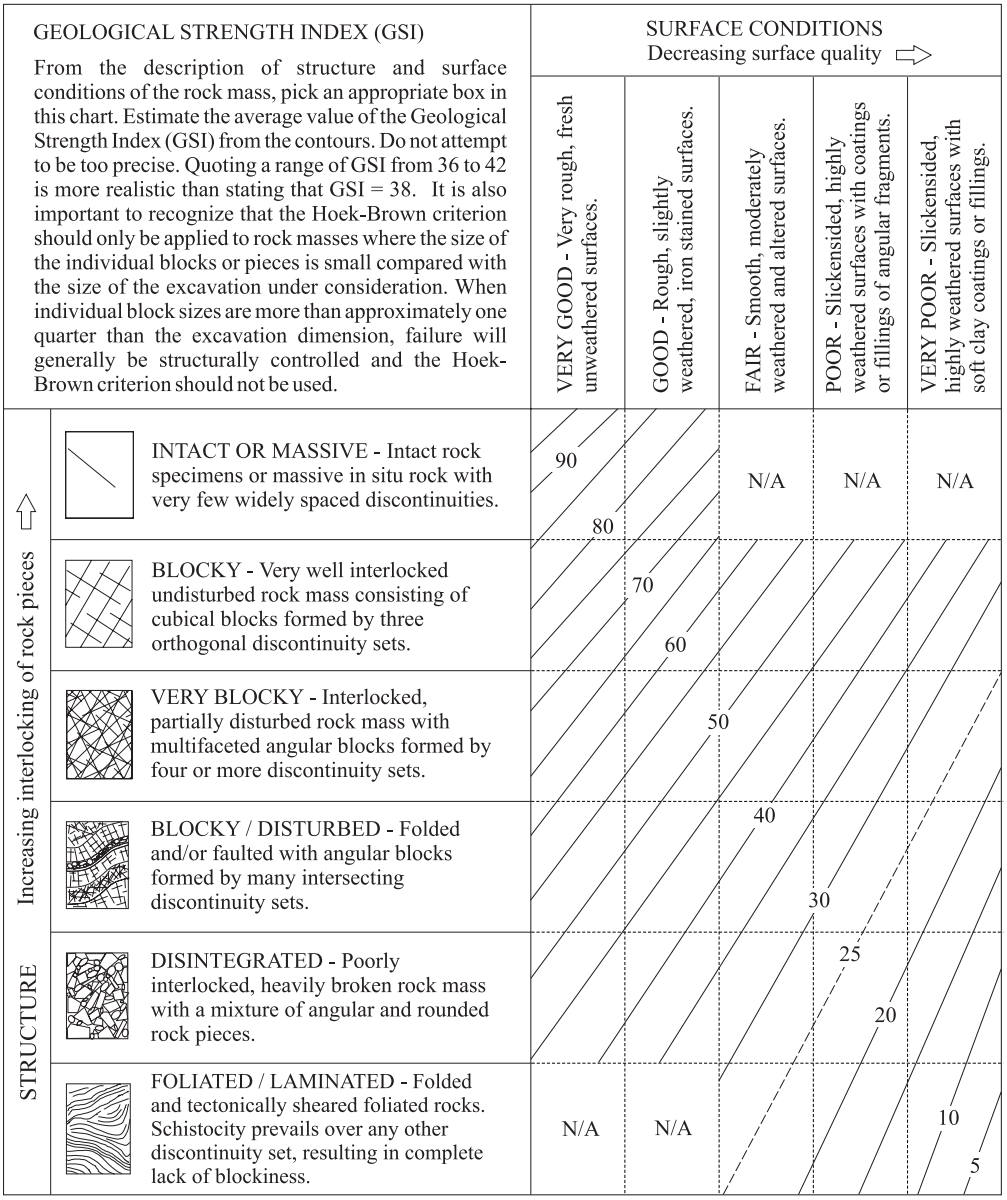

Figure B-3. Empirical chart for the estimation of the Geological Strength Index (GSI) based on the characteristics of the rock-mass [adapted from Hoek and Brown (1997) and Marinos and Hoek (2000)].

of equation (B-1), and the value of GSI, as defined by the equation

$$m_b = m_i \exp\left(\frac{GSI - 100}{28}\right) \tag{B-3}$$

The parameters s and a also depend empirically on the value of GSI as follows,

for $GSI \geq 25$,

$$\begin{aligned} s &= \exp\left(\frac{GSI - 100}{9}\right) \\ a &= 0.5 \end{aligned} \tag{B-4}$$

and for $GSI < 25$,

$$\begin{aligned} s &= 0 \\ a &= 0.65 - \frac{GSI}{200} \end{aligned} \tag{B-5}$$

Table B-2 lists the values of m_b, s and a obtained from equations (B-3), (B-4) and (B-5) for different values of GSI. It can be seen that when $GSI = 100$ (the hypothetical case in which the rock-mass has the same strength as the intact rock sample), the parameters are $m_b = m_i$, $s = 1$ and $a = 0.5$. With these values, the yield condition for the rock-mass, equation (B-2), and for the intact rock, equation (B-1), are the same.

GSI	m_b/m_i	s	a
100	1.00	1.00	0.5
75	40.95×10^{-2}	621.77×10^{-4}	0.50
50	16.77×10^{-2}	38.66×10^{-4}	0.50
25^+	6.87×10^{-2}	2.40×10^{-4}	0.50
25^-	6.87×10^{-2}	0.00	0.53
10	4.02×10^{-2}	0.00	0.60

Table B-2. Values of coefficients m_b, s and a as a function of the Geological Strength Index (GSI), computed from equations (B-3), (B-4) and (B-5) respectively. [Note that the second column represents ratio m_b/m_i; values of m_i for different rock types are given in Figure B-2.]

Londe (1988) showed that the Hoek-Brown failure criterion defined by equation (B-2) can be transformed into a 'general' failure envelope that is independent of the parameters σ_{ci}, m_b and s.

The transformation suggested by Londe applies to the particular case $a = 0.5$

and involves dividing the stress magnitudes by $m_b\sigma_{ci}$ and adding the term s/m_b^2. Considering the parameters introduced in equation (B-2), the scaled stresses S_1 and S_3 can be defined as,

$$S_1 = \frac{\sigma_1}{m_b\sigma_{ci}} + \frac{s}{m_b^2} \tag{B-6}$$

$$S_3 = \frac{\sigma_3}{m_b\sigma_{ci}} + \frac{s}{m_b^2} \tag{B-7}$$

With the stresses σ_3 and σ_1 replaced by the scaled stresses S_3 and S_1 from equations (B-6) and (B-7), the failure criterion for the rock-mass, equation (B-2), can be written in the form (Londe 1988)

$$S_1 = S_3 + \sqrt{S_3} \tag{B-8}$$

Note that in this 're-scaled' form of the failure criterion the parameters σ_{ci}, m_b and s are 'hidden' within the scaled stresses S_1 and S_3; the relationship applies then to any type of rock that is assumed to obey the Hoek-Brown criterion [12].

To illustrate the use of Londe's transformation, we will re-examine the triaxial test results for the samples of granite, quartz dolerite and marble presented in Figure B-1. Note that the results for intact rock samples can be equally approximated by equation (B-2), taking $GSI = 100$, and $s = 1$, $m_b = m_i$ and $a = 0.5$. Figure B-4 represents the scattered pairs (σ_3, σ_1) of Figure B-1 together with the Hoek-Brown failure criterion —equation (B-2) or (B-1)— plotted in terms of scaled principal stresses (i.e., with the axes representing the transformed stresses S_1 and S_3 defined by equations B-6 and B-7). It is seen that the stresses at failure for all three types of rocks align now to the 'general' form of the Hoek-Brown criterion defined by equation (B-8).

The use of equation (B-8) rather than equation (B-2) can lead to important simplifications in mechanical analyses involving the Hoek-Brown criterion. Carranza-Torres and Fairhurst (1999) have applied the transformation (B-8) in solving the problem of excavating cylindrical and spherical openings in rock-masses that satisfy the Hoek-Brown failure criterion. This solution is the basis for construction of Ground Reaction Curves in the Convergence-Confinement method discussed in the main text.

Just as the strength of the rock-mass is usually lower than the strength of the intact rock, the (elastic) deformation modulus of the rock-mass is also usually lower than that of the intact rock. Serafim and Pereira (1983) have proposed an empirical relationship to compute the deformation modulus of the rock-mass from the unconfined compressive strength of the intact rock sample and the value of the Rock Mass Rating (RMR) by Bieniawski (1976). Based on the original equation by Serafim and Pereira, Hoek and Brown (1997) propose the following relationship

[12] It should be emphasized though that the equation (B-8) is strictly valid only when the parameter a in equation (B-2) is equal to 0.5. According to equations (B-4) and (B-5), $a = 0.5$ for the broad range of situations in which $GSI \geq 25$.

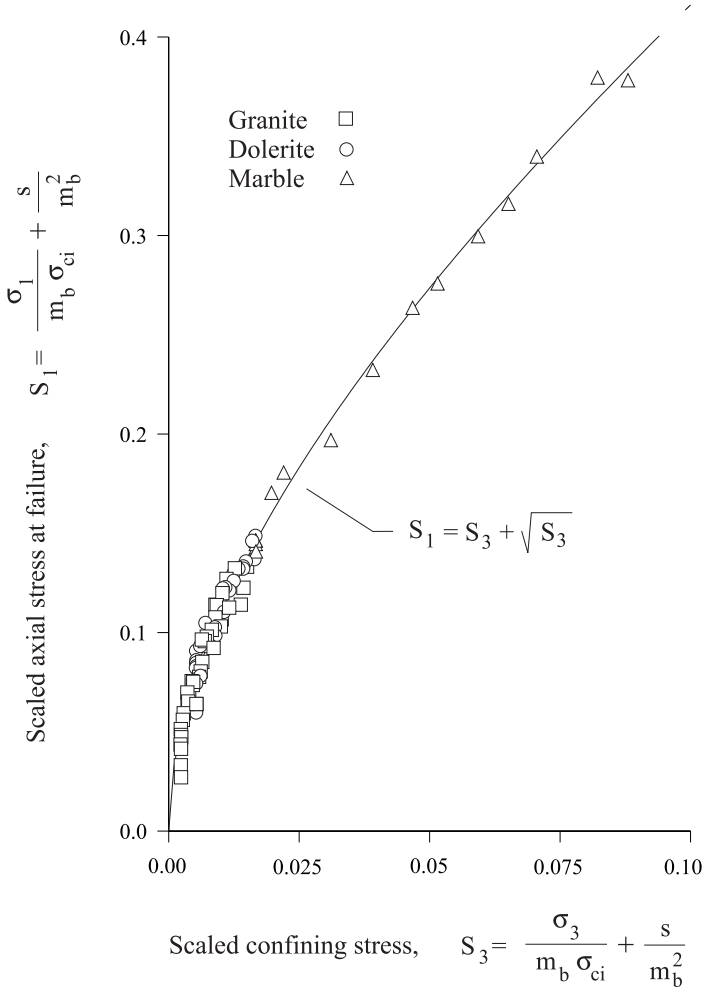

Figure B-4. Results from triaxial tests shown in Figure B-1 with the principal stress axes σ_1 and σ_3 normalized according to transformations (B-6) and (B-7). Note that in this reference system results for all three rock types fall on the 'general' failure envelope given by equation (B-8) [Londe (1988)].

between the rock-mass modulus E_{rm} and the Geological Strength Index *GSI*,

$$E_{rm} = 1000\ C\ (\sigma_{ci})\ 10^{\frac{\mathrm{GSI}-10}{40}} \tag{B-9}$$

where

$$\begin{aligned} C\ (\sigma_{ci}) &= 1 && \text{if} \quad \sigma_{ci} \geq 100\text{MPa} \\ &= \sqrt{\frac{\sigma_{ci}}{100}} && \text{if} \quad \sigma_{ci} < 100\text{MPa} \end{aligned}$$

In equation (B-9), both the unconfined compressive strength σ_{ci} and the rock-mass modulus E_{rm} are expressed in MPa.

In elasto-plastic analyses of deformations —such as the one presented in the main text— the rock-mass shear modulus G_{rm} is used rather than the deformation modulus E_{rm} given by equation (B-9). The shear modulus of the rock-mass can be estimated from the deformation modulus using the classic relationship from isotropic elasticity,

$$G_{rm} = \frac{E_{rm}}{2(1+\nu)} \tag{B-10}$$

In equation (B-10), ν is Poisson's ratio for the rock-mass, and is usually considered to vary between 0.1 and 0.3.

To illustrate the application of equations (B-9) and (B-10), let us consider the properties of the granite sample listed in Table B-1. The unconfined compressive strength of the intact rock is approximately $\sigma_{ci} = 141$ MPa; if the Geological Strength Index of the rock-mass is $GSI = 50$, then the deformation modulus of the rock-mass is, from equation (B-9), $E_{rm} = 1187$ MPa. If Poisson's ratio for the intact rock and rock-mass are both assumed to be equal to 0.22 then, from equation (B-10), the shear modulus of the rock-mass is $G_{rm} = 486$ MPa. The elastic constants E_{rm} and G_{rm} for the rock-mass are seen to be significantly lower than the corresponding constants E and G for the intact rock sample listed in Table B-1.